

DFVLR

Deutsche Forschungs- und
Versuchsanstalt
für Luft- und Raumfahrt

NASA-CR-176,604



Forschungsbericht

NASA-CR-176604
19860011251

Shear Layer Excitation, Experiment versus Theory

Dietrich W. Bechert and Bernhard Stahl

DFVLR
Institut für Experimentelle Strömungsmechanik
Göttingen
Abteilung Turbulenzforschung, Berlin

LIBRARY COPY

JUL 17 1986

LANGLEY RESEARCH CENTER
LIBRARY, NASA
LANGLEY STATION
HAMPTON, VIRGINIA

DFVLR-FB 84-26



NF00437

(Als Manuskript gedruckt)

Herausgegeben von
der Deutschen Forschungs- und Versuchsanstalt für Luft- und Raumfahrt e.V. (DFVLR),
Mitglied der Arbeitsgemeinschaft der Großforschungseinrichtungen (AGF).

Zu beziehen durch
Wissenschaftliches Berichtswesen der DFVLR
Postfach 90 60 58, 5000 Köln 90.

ISSN 0171-1342

DFVLR

Deutsche Forschungs- und
Versuchsanstalt
für Luft- und Raumfahrt



Forschungsbericht

Shear Layer Excitation, Experiment versus Theory

Dietrich W. Bechert and Bernhard Stahl

DFVLR

Institut für Experimentelle Strömungsmechanik
Göttingen

Abteilung Turbulenzforschung, Berlin

84 pages 40 figures 2 tables 23 references

DFVLR-FB 84-26

N86-20722#

Manuskript eingereicht am 30. Juli 1984

Stability, Aeroacoustics, Shear Layers, Jets

Dietrich W. BECHERT and Bernhard STAHL
Institut für Experimentelle Strömungsmechanik der DFVLR, Göttingen
Abteilung Turbulenzforschung, Berlin

Shear Layer Excitation, Experiment versus Theory

*DFVLR-Forschungsbericht 84-26, 1984, 84 pages, 40 figs., 2 tabs., 23 refs.,
21,50 DM*

The acoustical excitation of shear layers is investigated. Acoustical excitation causes, e.g., the so-called "orderly structures" in shear layers and jets. Also, the deviations in the spreading rate between different shear layer experiments are due to the same excitation mechanism. The present investigations focus on measurements in the linear interaction region close to the edge from which the shear layer is shed. Report is given on two sets of experiments (Houston 1981 and Berlin 1983/84). The measurements have been carried out with shear layers in air using hot-wire anemometers and microphones. The agreement between these measurements and the theory is good. Even details of the fluctuating flow field correspond to theoretical predictions, such as the local occurrence of negative phase speeds.

Stabilität, Aeroakustik, Scherschichten, Strahlen

(In englischer Sprache)

Dietrich W. BECHERT und Bernhard STAHL
Institut für Experimentelle Strömungsmechanik der DFVLR, Göttingen
Abteilung Turbulenzforschung, Berlin

Scherschicht-Anregung. Vergleich von Experiment und Theorie

*DFVLR-Forschungsbericht 84-26, 1984, 84 Seiten, 40 Bilder, 2 Tabellen,
23 Literaturstellen, 21,50 DM zzgl. MWSt*

Eine Scherschicht wird akustisch angeregt. Akustische Beeinflussungen dieser Art treten bei Scherschichten und Triebwerksstrahlen meistens auf und erklären die Existenz „geordneter Strukturen“. Die Unterschiede in der Ausbreitungsrate von Scherschichten bei verschiedenen Experimenten kommen ebenfalls durch akustische Anregung zustande. Die jetzigen Experimente konzentrieren sich auf den Bereich linearer Scherschichtbeeinflussung im Bereich der Abströmkante. Über zwei Reihen von Experimenten wird berichtet (Houston 1981 und Berlin 1983/84). Die Messungen wurden an Scherschichten in Luft mit Hitzdrahtanemometern und Mikrofonen ausgeführt. Die Übereinstimmung mit der Theorie ist gut und geht bis in Details des Wechselströmungsfeldes, wie etwa das lokale Auftreten von negativen Phasengeschwindigkeiten.



Shear Layer Excitation, Experiment versus Theory *)

Deutsche Forschungs- und Versuchsanstalt für Luft- und Raumfahrt
Forschungsbereich Strömungsmechanik
Institut für Experimentelle Strömungsmechanik
Abteilung Turbulenzforschung
Müller-Breslau-Straße 8, D-1000 Berlin (West) 12

Berlin, im März 1984

Komm. Forschungsbereichsleiter:

Prof. Dr.rer.nat. H.L. Jordan

Institutsleiter:

Prof. H. Hornung, Ph.D.

Abteilungsleiter:

Dr.-Ing. E. Pfizenmaier

Verfasser:

Dr.-Ing. D.W. Bechert

Dipl.-Ing. B. Stahl

*) Supported by NASA Lewis Research Center Grant NAG 3-198 (1981)
and by the Deutsche Forschungsgemeinschaft Grant Be 889/1-1
(1982-84).

Shear Layer Excitation, Experiment versus Theory

Summary

The acoustical excitation of shear layers is investigated. Acoustical excitation causes, e.g., the so-called "orderly structures" in shear layers and jets. Also, the deviations in the spreading rate between different shear layer experiments are due to the same excitation mechanism. The present investigations focus on measurements in the linear interaction region close to the edge from which the shear layer is shed. We report on two sets of experiments (Houston 1981 and Berlin 1983/84). The measurements have been carried out with shear layers in air using hot wire anemometers and microphones. The agreement between these measurements and the theory is good. Even details of the fluctuating flow field correspond to theoretical predictions, such as the local occurrence of negative phase speeds.

Stabilität, Aeroakustik, Scherschichten, Strahlen

Scherschicht-Anregung. Vergleich von Experiment und Theorie

Übersicht

Eine Scherschicht wird akustisch angeregt. Akustische Beeinflussungen dieser Art treten bei Scherschichten und Triebwerksstrahlen meistens auf und erklären die Existenz "geordneter Strukturen". Die Unterschiede in der Ausbreitungsrate von Scherschichten bei verschiedenen Experimenten kommen ebenfalls durch akustische Anregung zustande. Die jetzigen Experimente konzentrieren sich auf den Bereich linearer Scherschichtbeeinflussung im Bereich der Abströmkante. Über zwei Reihen von Experimenten wird berichtet (Houston 1981 und Berlin 1983/84). Die Messungen wurden an Scherschichten in Luft mit Hitzdrahtanemometern und Mikrofonen ausgeführt. Die Übereinstimmung mit der Theorie ist gut und geht bis in Details des Wechselströmungsfeldes, wie etwa das lokale Auftreten von negativen Phasengeschwindigkeiten.

<u>Contents</u>	page
1. Introduction.....	7
2. Relevant facts from theory.....	9
2.1. Basic assumptions.....	9
2.2. Excitation field.....	11
2.3. Velocity distributions, one stream case.....	15
2.4. Velocity distributions, two stream case.....	20
3. Short information on the facility.....	21
4. Mean flow field.....	23
5. Excitation sound field.....	27
6. Interaction measurements.....	32
6.1. Extrapolated field data.....	32
6.2. Direct comparison of the field data.....	35
6.3. Phase measurements.....	42
6.4. Measurements at higher Strouhal numbers.....	45
7. Conclusions.....	49
8. References.....	52
9. Appendices.....	55
9.1. Appendix A: Glossary of symbols.....	55
9.2. Appendix B: Experimental apparatus.....	59
9.2.1. Facility Houston.....	59
9.2.2. Facility Berlin.....	62
9.2.3. Boundary layer suction.....	69
9.2.4. Vibration system.....	72
9.2.5. Background noise.....	78
9.3. Appendix C: Typing errors of DFVLR-FB 82-23.....	83

1. Introduction

The fact that sound waves cause wavelike perturbations and orderly vortex formations in shear layers and jets has been known for at least one hundred years [1,2]. Even excellent photographs of shear layers demonstrating the evolution of vortices are available for more than fifty years, see Fig. 1.

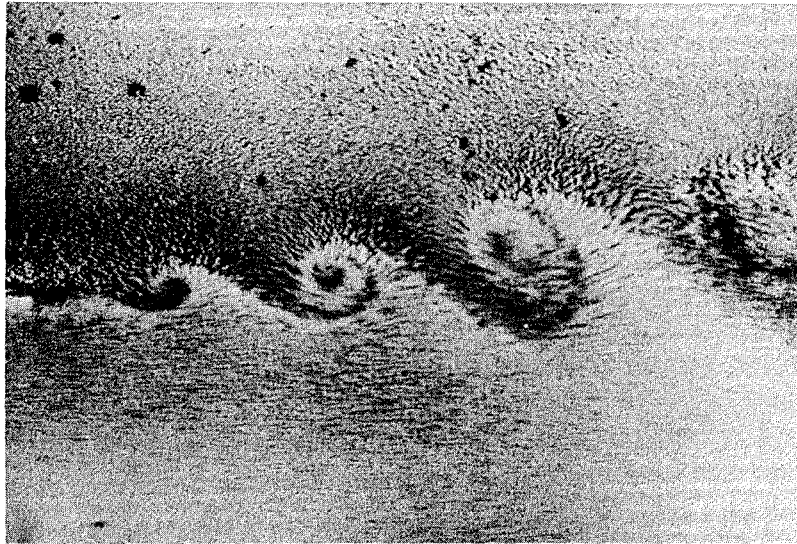


Fig. 1 Roll-up process in a shear layer. Photograph taken by F. Michel, 1932 [3].

Observations on excited jets led to the development of the stability theory of flows by Lord Kelvin, von Helmholtz and Lord Rayleigh. The interest of theoreticians in the following century was concentrated on determining the limits of the stability of flows and on the evolution of the instability waves including their nonlinear development.

On the other hand, little attention had been paid to the understanding of the initial observations, i.e., that instability waves in shear layers are tied to acoustical waves. During the last decade, it was demonstrated that also turbulent flows can

be dominated by instability waves and the subsequent evolution of turbulent vortices [4]. Also, the significance of acoustic excitation became evident in turbulent shear flows, as it was in the analogous case of laminar shear layers [5,6]. Moreover, the observation that the broad band noise emission of turbulent jets can be enhanced by acoustical tone excitation [7,8,9] has increased interest in the forcing mechanism of instability waves.

Thus, a small number of theoretical papers on acoustical shear layer excitation has emerged in the past ten years [10-13]. Unfortunately, these papers did not produce results which were easily verifiable by experimentalists. In addition, there was no guideline on what the relevant quantities to be measured were, and how to proceed in such an experiment. One of the authors (D.W.B.) tried to produce the necessary theoretical data in a preceding report [14]. The present experimental investigation aims at verifying this theoretical material.

We provide here two sets of data taken in different institutes. The first set was taken in 1981 by D.W. Bechert at the University of Houston, Tx., U.S.A.. However, it was suspected that these data might have been slightly contaminated by systematic errors caused, e.g., by:

- (i) overshoot of the mean velocity profile at the shear layer,
- (ii) too high vibration levels in the facility which caused problems with the vibration sensitivity of the microphones,
- (iii) partly unreliable electronic instruments, such as a beat frequency oscillator, which did not keep the excitation frequency sufficiently constant.

Subsequently, the major possible error sources were scrutinized and it was concluded that the Houston data were at least of value in suggesting that the theory is correct. Thus, some data were published in 1983 [15].

A second facility was then established in Berlin. The new data taken by B. Stahl and D.W. Bechert were much more reliable and reproducible. On the other hand, it turned out, that only very few of the previous (Houston) data had to be rejected, and none of the published ones. In hindsight, it might appear that we were overscrupulous to carry out an experiment twice. However, the issue of shear layer excitation is so much confused by lacking thoroughness of previous authors, that it seemed worthwhile to have this double effort to solve the problem.

2. Relevant facts from theory

2.1. Basic assumptions

We outline here the basic assumptions of the theory and the theoretical results from our previous report [14] relevant for this experimental investigation. The following simplifying assumptions had been introduced in the theory:

1. plane flow
2. all fluctuating quantities harmonic in time, i.e., $\propto e^{-i\omega t}$
3. linearized problem
4. incompressible flow
5. parallel mean flow
6. inviscid flow
7. infinitesimally thin shear layer.

The assumptions (1) and (2) can be fulfilled easily in an experiment. The perturbation velocities should be small in comparison to the mean flow velocity so that linearity is still maintained (3). Linearity can be also checked directly in the experiment. This can be done by varying the excitation level and by observing the velocity fluctuations in the region of the highest fluctuations in the shear layer. If excitation level and velocity fluctuations are proportional, the system is linear. This linearity, however, applies only to a certain region downstream of the splitter plate edge. Beyond this linearity regime no data were taken in our experiments. The condition of incompressibility (4) can be maintained, at least for the interaction

region downstream of the splitter plate, if the Mach number is small, as shown in our theoretical report [14]. If we want to calculate the pressure distribution of the excitation field we can use incompressible flow theory (such as conformal mapping) if the acoustic wavelength is large compared to the typical dimension of the test section, i.e., the channel width of our facility. Conditions (5) to (7) are related to viscosity effects. Parallel mean flow (5) is reasonable to assume for a laminar shear layer if the Reynolds number is not too low. The condition of inviscid flow (6) has been shown to work remarkably well if, again, the Reynolds number is not too low [16,17]. The strongest restriction is the condition of an infinitesimally thin shear layer (7). Consequently, we can expect a good agreement between the theory [14] and our measurements only at low Strouhal numbers, where the wavelength of the perturbations is large compared to the thickness of the shear layer. We can assume that deviations will occur where the conventional stability theory *) predicts deviations (in spatial amplification rate and wave number) between a simple step velocity profile, with thickness zero, and a real shear layer velocity profile. If we consider Michalke's theoretical results [16], see Fig. 2, we expect the onset of deviations at a Strouhal number, say, between $S_\theta = 0.003$ and $S_\theta = 0.005$. It should be mentioned that the Strouhal number $S_\theta = f \cdot \theta / \bar{U}_2$ is calculated with the momentum thickness θ of the shear layer velocity profile (therefore, the actual numbers of S_θ are comparatively small). f is the excitation frequency and \bar{U}_2 is the mean flow velocity.

Michalke's calculations in Fig. 2 have been carried out for a mean velocity profile with the shape of a hyperbolic tangent function. The magnitude growth of the instability waves is proportional to $e^{\lambda_r x}$ in the downstream direction x . λ_i is the wave number of the instability waves. The relation to the more common symbols α_i and α_r is also given in Fig. 2.

*) The term "conventional stability theory" means calculations on shear layers with properties invariable in the streamwise direction, i.e., parallel mean flow and the shear layer being extended from minus infinity to plus infinity.

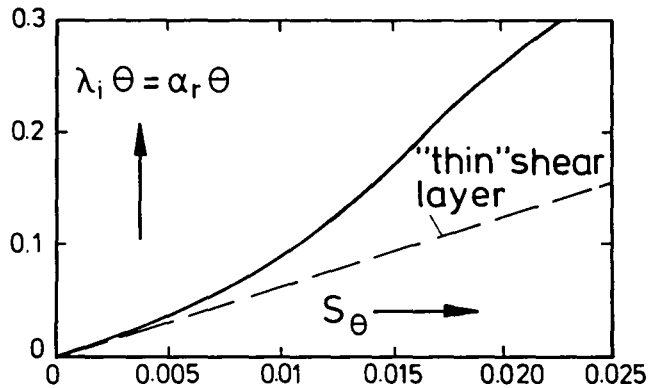
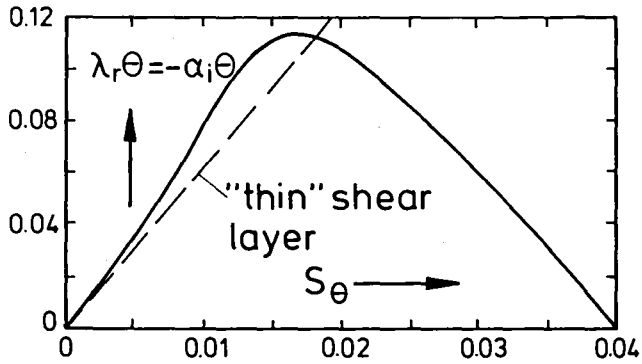


Fig. 2 Amplification rate ($\lambda_r \theta$) and wave number ($\lambda_i \theta$) of a shear layer with finite thickness [16].

2.2. Excitation field

One of the most relevant ideas in our previous theory [11,14,15] is the concept of field decomposition. The fluctuating field is split into one contribution produced by the exterior forcing (excitation field) and another produced by the shear layer per-

turbation. Both together fulfill the conditions of equal pressure and equal displacement on both sides of the shear layer. The excitation pressure is transmitted through the shear layer and hence this pressure contribution is antisymmetrical with respect to the shear layer. The pressure contribution from the shear layer itself, on the other hand, is symmetrical with respect to the shear layer, see Fig. 3.

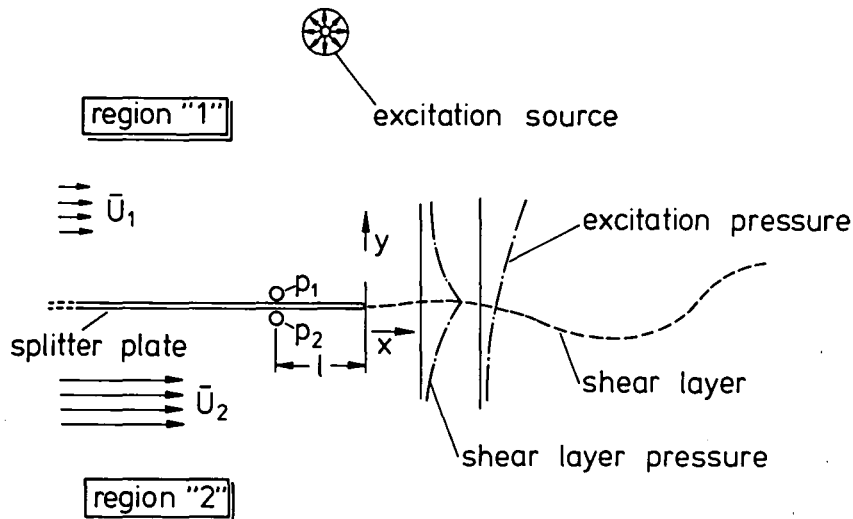


Fig. 3 Field decomposition in antisymmetrical (excitation) and symmetrical (shear layer) parts of the pressure field.

If we consider the most common case of an excitation, where the source is not too close to the trailing edge of the splitter plate, we find an excitation field which is parabolic (see Fig. 4).

The distribution of this (instantaneous) excitation pressure field can be determined by conformal mapping [14]. Its magnitude can be found experimentally by measuring the pressure difference $p_1 - p_2 = \Delta p_{12}$ on both sides of the splitter plate, not too far upstream of the trailing edge. The relevant quantity of the

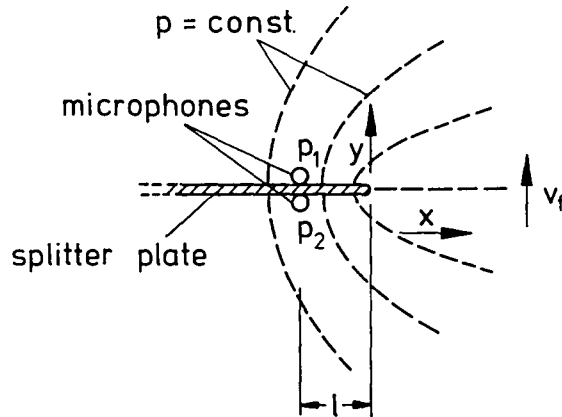


Fig. 4 Instantaneous parabolic field of the exterior excitation.

excitation field is the forcing velocity v_f perpendicular to the shear layer. It is proportional to the pressure difference Δp_{12} and obeys the following law [14]:

$$(1) \quad v_f = -i \cdot \frac{\Delta p_{12}}{4\rho\omega\sqrt{l}} \cdot \frac{1}{\sqrt{x}}.$$

The coefficient i corresponds to a 90° phase shift in comparison to the phase of Δp_{12} . l is the distance of the microphones (to measure Δp_{12}) from the trailing edge of the splitter plate. We find that v_f is proportional to $1/\sqrt{x}$. This produces a singularity of v_f at $x = 0$. However, the complete flow field does not have any singularities at the trailing edge [14].

There is a deviation from the $1/\sqrt{x}$ law if the splitter plate is located in the center of a channel. This arrangement is typical for experiments, because one can produce only streams with finite width. For a calculation of this, more realistic case we assume that the sound sources are located in the channel far upstream of the trailing edge of the splitter plate. If the sound wave-

length of the excitation is much larger than the channel width, the problem can be solved analytically by conformal mapping [14]. The result differs slightly from equation (1), i.e.,

$$(2) \quad v_f = -i \cdot \frac{\Delta p_{12}}{4\rho\omega\sqrt{l}} \cdot \frac{\sqrt{\pi/d}}{\sqrt{e^{\pi x/d} - 1}} .$$

In this equation $2d$ is the width of the channel. We find that the field is still parabolic in the vicinity of the plate edge, but it decays more rapidly in the downstream direction.

To plot the data of v_f , measured in a channel, we may use a dimensionless form. Since these data are taken in air at rest with the mean velocity $\bar{U}_2 = 0$ we cannot use any reference velocity which contains this quantity. If we assume, hypothetically, a sound excitation far upstream in the channel, we can use the fluctuating velocity there, u_∞ . It has the value [14]:

$$(3) \quad u_\infty = \frac{|\Delta p_{12}|}{4\rho\omega\sqrt{l}} \cdot \sqrt{\pi/d} .$$

With that reference velocity, we may write eq. (2) for convenience *)

$$(4) \quad \boxed{\frac{|v_f|}{u_\infty} = \frac{1}{\sqrt{e^{\pi x/d} - 1}}} .$$

In an experiment, it is also possible to determine directly the value of v_f and its relation to the excitation pressure difference Δp_{12} . For this purpose we take measurements with only the

*) Throughout this paper, a quantity between vertical bars like, e.g., $|v_f|$ means the modulus or peak value of this quantity during one cycle of a sinusoidal vibration.

excitation sound field switched on. In the vicinity of the plate edge we produce under almost all conceivable excitation conditions a standing pressure field. The local fluctuating pressure can be measured with a pressure probe with a typical resolution of $1 \pm 1,5$ mm. We can measure, e.g., the pressure $|p|$ as a function of y in sections of $x = \text{const}$. The gradient $\partial|p|/\partial y$, which can be evaluated graphically at $y=0$, allows to determine v_f by using the Euler equations. We find

$$(5) \quad |v_f| = \frac{1}{\rho \omega} \cdot \frac{\partial |p|}{\partial y} \quad (y=0) \cdot$$

The evaluation of the real distribution of v_f in the test section as compared to equations (1) and (2) will be shown in section 5 of this paper.

2.3. Velocity distributions, one stream case

With mean flow switched on, we have an interaction between excitation field and shear layer. The theory for this interaction is explained extensively in our previous publications [11,14,15]. First, we provide here the solutions for the one stream case where the mean flow velocity above the shear layer is zero ($\bar{u}_1 = 0$). For the resulting v velocity perpendicular to the mean flow and just above the shear layer in the fluid at rest we find a general solution [14]:

$$(6) \quad v_1 = -\frac{\omega}{\bar{u}_2} e^{\lambda_1 x} \int_0^x e^{-\lambda_1 x} v_f dx + \frac{\omega}{\bar{u}_2} e^{\lambda_2 x} \int_0^x e^{-\lambda_2 x} v_f dx$$

with

$$(7) \quad \lambda_1 = \frac{\omega}{\bar{u}_2} (i+1) \quad ; \quad \lambda_2 = \frac{\omega}{\bar{u}_2} (i-1) \cdot$$

If we insert v_f from eq. (1) we obtain

$$(8) \quad v_1 = i \cdot \frac{\sqrt{\pi}}{4} \cdot \frac{\Delta p_{12}}{\rho \sqrt{\bar{u}_2 \omega l}} \cdot \left[\frac{e^{\lambda_1 x}}{\sqrt{i+1}} \operatorname{erf} \sqrt{\lambda_1 x} - \frac{e^{\lambda_2 x}}{\sqrt{i-1}} \operatorname{erf} \sqrt{\lambda_2 x} \right] \cdot$$

The expression $\text{erf } \sqrt{\lambda_1 x}$ becomes unity for $\omega x / \bar{U}_2 \gg 1$, and the second expression in the brackets of eq. (8) vanishes for $\omega x / \bar{U}_2 \gg 1$ because it is exponentially decaying. So we have for the mean value of v_1 :

$$(9) \quad |v_1| \approx \frac{\sqrt{\pi}}{4 \cdot \sqrt{2}} \cdot \frac{|\Delta p_{12}|}{\rho \sqrt{\bar{U}_2 \omega l}} \cdot e^{\omega x / \bar{U}_2}, \text{ for } \omega x / \bar{U}_2 \gg 1.$$

In fact, this equation is already valid above $\omega x / \bar{U}_2 \approx 1.5$. The quantity $|\Delta p_{12}| / \rho \sqrt{\bar{U}_2 \omega l}$ has the dimension of a velocity and may be used as a new reference velocity of the excitation

$$(10) \quad \boxed{u_{\text{ref}} = \frac{|\Delta p_{12}|}{\rho \sqrt{\bar{U}_2 \omega l}}}$$

On the other hand, it is also convenient to divide all fluctuating quantities by this reference velocity to obtain dimensionless quantities, like

$$(11) \quad \tilde{v}_1 = v_1 / u_{\text{ref}} ; \tilde{u}_1 = u_1 / u_{\text{ref}}.$$

In addition, it is useful to introduce dimensionless length scales in the form of Strouhal numbers, namely

$$(12) \quad \tilde{x} = x \omega / \bar{U}_2 ; \tilde{y} = y \omega / \bar{U}_2.$$

Hence, equation (9) becomes quite simple

$$(13) \quad |\tilde{v}_1| \approx \frac{\sqrt{\pi}}{4 \cdot \sqrt{2}} \cdot e^{\tilde{x}}.$$

However, equations like (8), (9) or (13) cannot be verified easily, because it is very difficult to measure small v-velocity components in a mean flow \bar{U} (in x-direction). It is much more convenient to measure accurately fluctuating u-velocities with,

e.g., a hot wire probe. In addition, it is also preferable to take hot wire measurements in a region with mean flow (region "2" in Fig. 3 below the shear layer with $y \leq 0$) rather than in a fluid at rest. For the fluctuating u-velocity at $y = -0$, just below the shear layer, the theory [14,15] provides a very simple analytic solution *), i.e.,

$$(14) \quad \tilde{u}_2|_{y=-0} = -i \cdot \frac{\sqrt{\pi}}{4} \left[\frac{e^{\lambda_1 x}}{\sqrt{i+1}} + \frac{e^{\lambda_2 x}}{\sqrt{i-1}} \right]$$

with the modulus

$$(15) \quad \boxed{|\tilde{u}_2|_{y=-0} = \frac{\sqrt{\pi}}{4 \cdot \sqrt[4]{2}} \cdot \sqrt{e^{2\tilde{x}} + e^{-2\tilde{x}} + \sqrt{2}}}$$

Unfortunately, again this velocity cannot be measured directly. The real fluctuating velocities inside the shear layer cannot be predicted by a theory for an infinitesimally thin shear layer. There is, however, a way to extrapolate the experimental data taken outside of the shear layer to obtain the value of $|\tilde{u}_2|$ at $y = -0$. We plot the data measured in the potential field outside the shear layer on logarithmic paper and extrapolate linearly towards the center of the shear layer (see Fig. 5). This procedure should work at least for locations farther downstream, where we expect an exponential decay in y-direction of the instability waves.

The data in our previous publication [15] and in section 6.1. of this report are evaluated with this procedure. The technique is useful to plot our numerous data, but it has also its limitations. This will become evident, if we consider numerically calculated distributions of $|\tilde{u}_2|$. Such data had been provided in our theory

*) Eq. (14) is mistyped in our theory report [14], the negative sign had been omitted. A list of typing errors of this report [14] is given in the appendix.

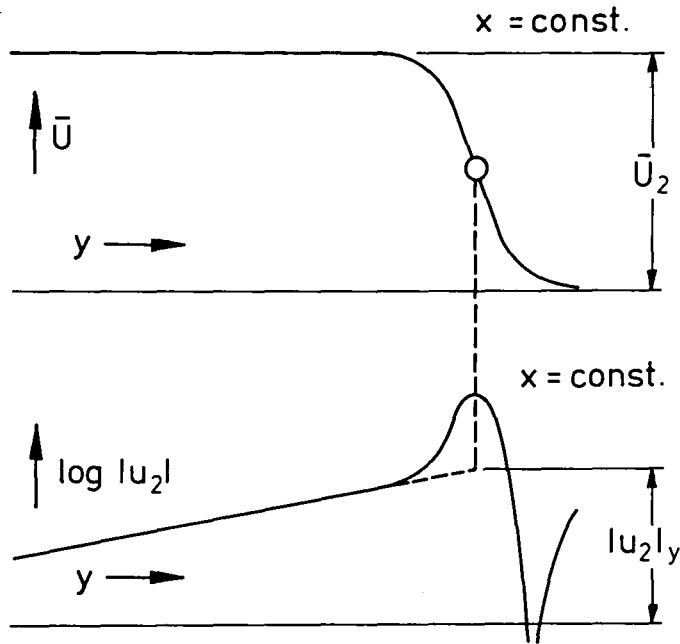


Fig. 5 Mean flow velocity profile and logarithmic plot of the fluctuating velocity $|u_2|$ with extrapolation.

report [14]. Fig. 6 shows these theoretical data for various distances \tilde{x} upstream and downstream of the splitter plate edge. From Fig. 6 we see, that an extrapolation for $y = -0$ at small \tilde{x} produces too low values of $|\tilde{u}_2|_{y = -0}$. At sufficient distance, say, at $\tilde{x} > 0.5$ the extrapolation is valid, though.

A direct comparison between measurements and computed values, like in Fig. 6, is more conclusive and it will be also carried out for one series of data.

As we have seen in section 2.2., the acoustical excitation does not produce under all circumstances a $1/\sqrt{x}$ law for the forcing velocity v_f (see eq. (1)). It may deviate by the existence of channel walls and may decay, therefore, more rapidly in the downstream direction, see eq. (2). An estimation of this in-

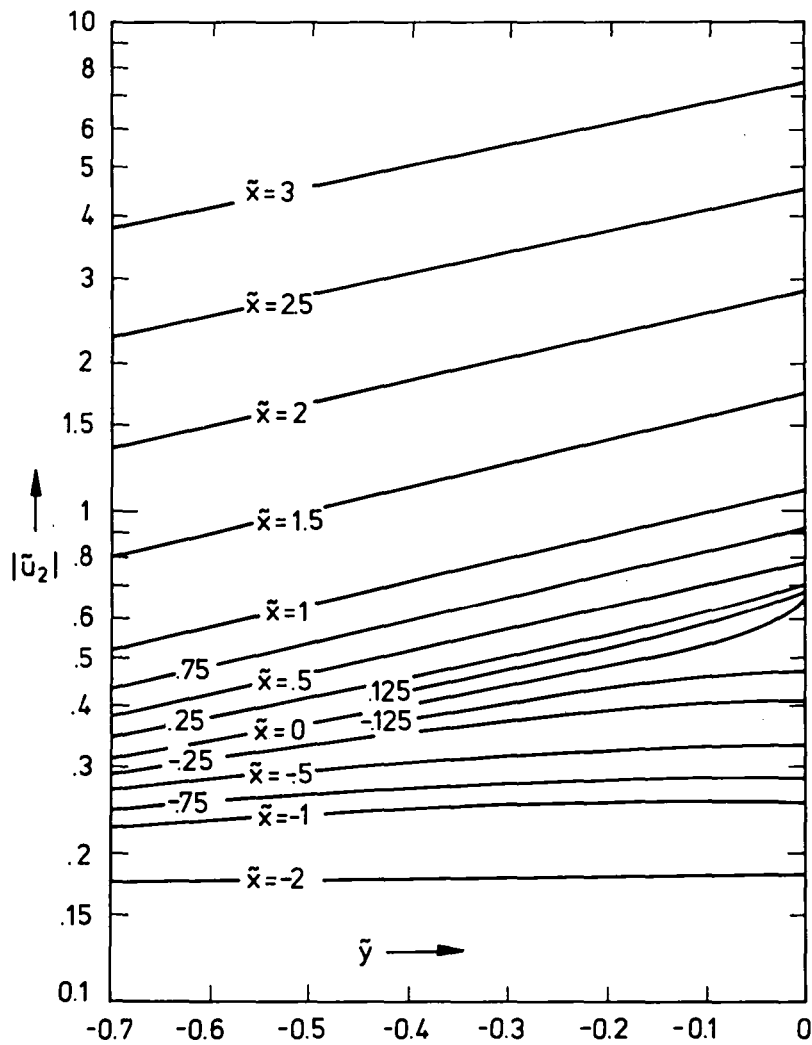


Fig. 6 Computed values of $|\bar{u}_2|$ in the mean flow region $\tilde{y} \leq 0$, from [14].

fluence can be also found in our theory report [14]. The magnitude of the shear layer fluctuations decreases by a coefficient

$$(16) \quad c = \left(1 - \frac{\pi}{16} \cdot \frac{\bar{U}_2}{\omega d}\right) .$$

However, as an influence of the finite channel width $2d$ this plays only a rôle for the Houston data. For the lowest Strouhal number, we obtain there a fluctuation magnitude decreased by 11.2 %. For the higher Strouhal numbers, this has no perceivable effect anymore.

2.4. Velocity distribution, two stream case

There is still another basic difference between the theoretical results displayed so far and an experimental situation. In an experiment with a shear layer located in a channel, the mean flow velocity in the region $y > 0$ above the shear layer (see Fig. 3) cannot be kept zero. If it were zero, the entrainment of the shear layer would produce a significant recirculation in the region $y > 0$, and also the shear layer itself would be deflected. Thus, in the present experiments, the mean flow velocity \bar{U}_1 above the shear layer was 10 % of the mean flow velocity \bar{U}_2 below the shear layer. So we have the velocity ratio σ :

$$(17) \quad \sigma = \bar{U}_1 / \bar{U}_2 = 0.1 .$$

The presence of the second stream changes the distribution of the fluctuating field slightly. In our theory report [14] we have also considered this case. We find for \tilde{u}_2

$$(18) \quad \tilde{u}_{2,y=0} = -i \cdot \frac{\sqrt{\pi}}{4(1+\sigma^2)} \cdot \left[\frac{1+i\sigma}{\sqrt{\lambda_1}} \cdot e^{\tilde{\lambda}_1 \tilde{x}} + \frac{1-i\sigma}{\sqrt{\lambda_2}} \cdot e^{\tilde{\lambda}_2 \tilde{x}} \right]$$

with

$$(19) \quad \lambda_{1,2} = \frac{1}{1+\sigma^2} [i(1+\sigma) \pm (1-\sigma)]$$

and with $\tilde{x} = \omega x / \bar{U}_2$, as before. Also the reference velocity, given by eq. (10), remains the same. For the modulus $|\tilde{u}_2|$ we

can derive from eq. (18)

$$(20) \quad |\tilde{u}_2|_{y=0} = \frac{\sqrt{\pi}}{4\sqrt{2(1+\sigma^2)}} \times \\ \times \sqrt{e^{2(1-\sigma)\tilde{x}} + e^{-2(1-\sigma)\tilde{x}} + 2\cos\left(\frac{\pi}{2} + 2\arctg\sigma - \arctg\left(\frac{1+\sigma}{1-\sigma}\right)\right)}$$

This boils down to

$$(21) \quad \boxed{|\tilde{u}_2|_{y=0} = 0.372 \sqrt{e^{1.8\tilde{x}} + e^{-1.8\tilde{x}} + 1.266}} \quad \text{for } \sigma = \bar{U}_1/\bar{U}_2 = 0.1.$$

Eq. (21) produces values of $|u_2|$ lower than eq. (15). The comparison with the experiments will also show a better agreement. We do not possess, however, any computed field data like for the case $\sigma = \bar{U}_1/\bar{U}_2 = 0$. Nevertheless, from our understanding of the interaction process we can assume, that for $\tilde{x} < 0$ the excitation field will dominate, so the values of \tilde{u}_2 for the two cases should not differ significantly there. For distances $\tilde{x} > 1$ the instability wave should dominate. Here, the decay in \tilde{y} -direction should be enhanced by the coefficient $(1+\sigma)/(1+\sigma^2)$ due to the fact that the wave number in \tilde{x} -direction is increased by this coefficient. This follows from a consideration of the induced velocity field of an infinitely extended instability wave. Or, roughly speaking, a wave field propagating in x -direction with wave number α decays exponentially with $e^{-|\alpha y|}$ in the y -direction. This latter consideration allows at least to estimate the distribution of $|\tilde{u}_2|$ for $\sigma = 0.1$ if it is known for $\sigma = 0$, the one stream case.

3. Short information on the facility

Fig. 7 shows the test section of the experimental setup. The splitter plate in the center of a rectangular channel separates the mean flow region ($\bar{U}=\bar{U}_2$ at $y<0$) from a region of very slow entrainment flow ($\bar{U}_1 \approx 0.1\bar{U}_2$ at $y>0$). The initial shear layer

thickness can be controlled by boundary layer suction through a slit in the splitter plate near the plate edge.

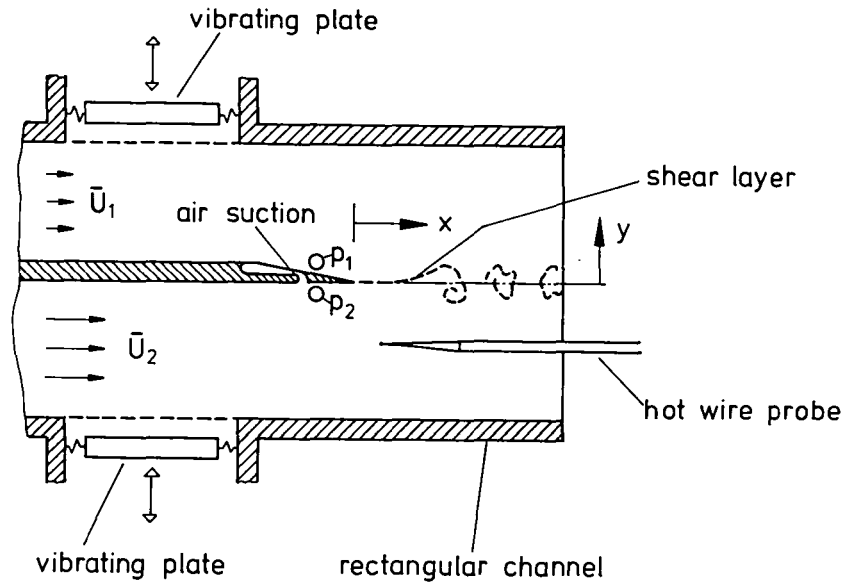


Fig. 7 Experimental arrangement.

The excitation is provided by two vibrating plates driven electromagnetically and adjusted in antiphase so that a surging motion around the edge of the splitter plate is produced. The magnitude of the excitation field is measured by two microphones on both sides of the splitter plate. The pressure difference $p_1 - p_2 = \Delta p_{12}$ is a direct measure for the acoustic excitation.

In order to prevent effects of the suction slit on the sound field, the oscillating flow through the slit can be compensated acoustically by a piston speaker in the suction duct. This piston speaker can be adjusted in magnitude and phase so that zero oscillating flow condition through the slit is achieved. This is checked by a second hot wire probe (not shown in Fig.7) inserted into the slit. In this way, the suction slit can be sealed acoustically.

We think, that this short information is sufficient to understand the measured data in the following sections. On the other hand, it cannot be understood how comparatively involved these measurements really are without reading the more detailed description of the experimental apparatus in the appendix: The flavour of the project can be appreciated much better if one knows explicitly where we used, e.g., the following items:

- (i) lady's stockings
- (ii) coffee sifters
- (iii) an empty barrel
- (iv) a garden hose
- (v) a vacuum cleaner.

4. Mean flow field

The data in this investigation had been taken under 4 different mean flow conditions, i.e., mean flow velocity 6 m/s or 12 m/s with boundary layer suction *) off or on. For each data set, Houston 1981, and Berlin 1983/84, the mean velocity distributions have been measured (see Figs. 8 and 9).

The Houston data show a little overshoot in the potential flow region, which is due to an interaction between screen and nozzle (see also appendix, section 9.2.1.). If we consider the differences between measurements without and with boundary layer suction, we see that

- (i) indeed, the boundary layer suction decreases the initial shear layer thickness effectively, and
- (ii) on the other hand, farther downstream, the shear layer spreading rate is increased.

*) Suction rate: 28.3 l/min (Houston) and 34.0 l/min (Berlin). The rate was the same for 6 m/s and 12 m/s mean velocity. The splitter plate breadth was 100 mm in both facilities.

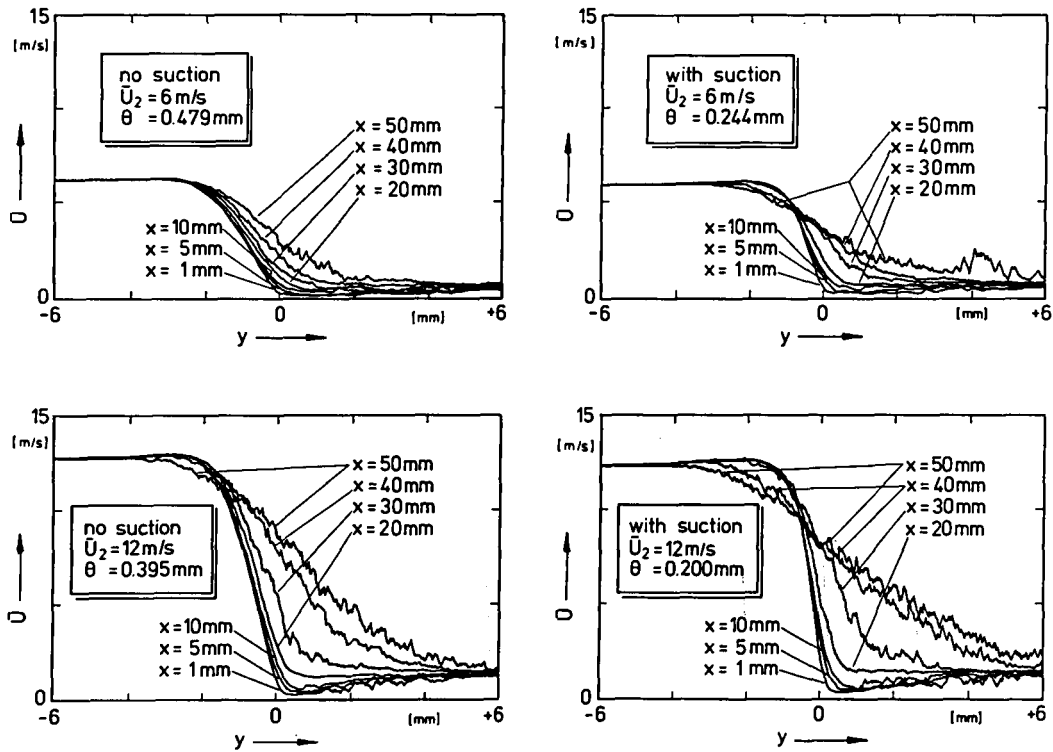


Fig. 8 Mean flow distribution (Houston 1981).

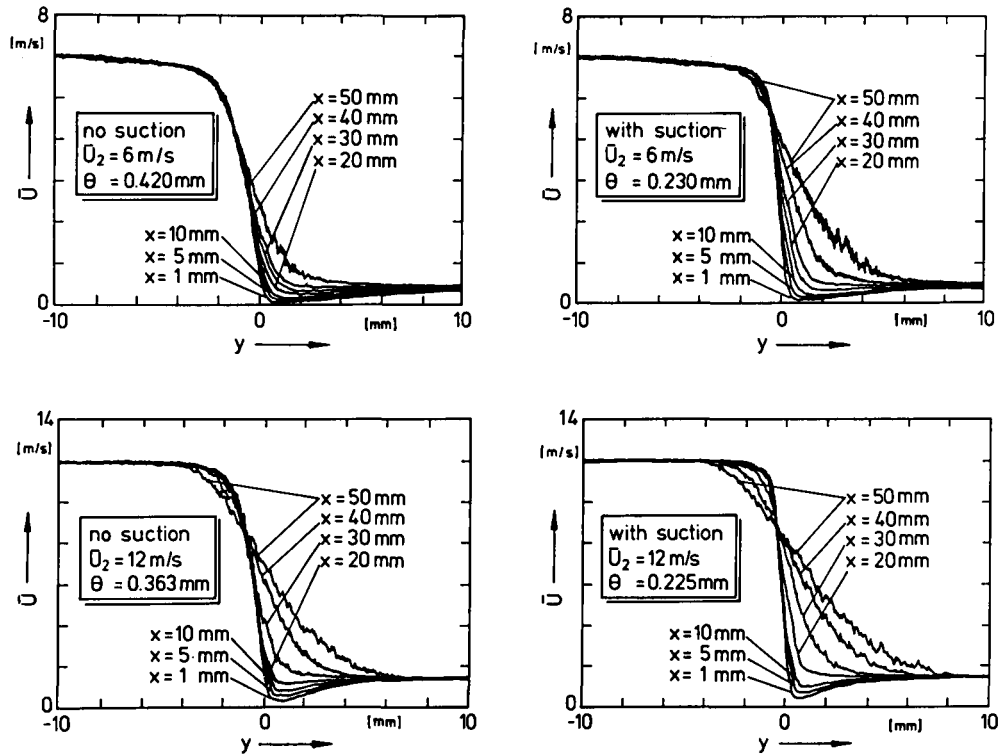


Fig. 9 Mean flow distribution (Berlin 1983/84).

Thus, the boundary layer suction produces a smaller shear layer thickness only over a certain downstream distance. In addition, we see that it is hard to define a meaningful shear layer thickness θ . The situation becomes even more complex, if we consider the splitter plate wake which is in particular visible for the Berlin measurements (where we have no turbulent separation at the splitter plate like in the Houston data). A definition (see also Fig. 10) like

$$\theta_1 = \int_{-\infty}^{+\infty} \frac{\bar{u}(y) - \bar{u}_1}{\bar{u}_2 - \bar{u}_1} \cdot \left(1 - \frac{\bar{u}(y) - \bar{u}_1}{\bar{u}_2 - \bar{u}_1} \right) dy$$

would lead, with the present data, to a momentum thickness which always varies with x . On the other hand, we would prefer to have a simple reference quantity for the shear layer thickness. A quantity, however, which does not vary very much within the first 15 mm downstream of the plate edge is the slope of the mean velocity profile. Therefore, we use a definition which, admittedly, is not very sophisticated, but appeared to be suitable (see Fig. 10).

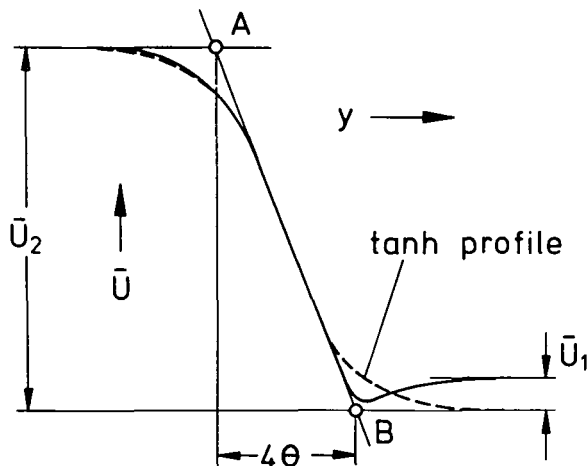


Fig. 10 On the definition of θ .

- (i) we determine the slope of the initial profile at, say, $x=1\text{mm}$, where the slope is still identical with that of the plate boundary layer
- (ii) we replace the real velocity profile with a hyperbolic tangent profile of the same slope
- (iii) we determine the points A and B where the slope line intersects with the lines $\bar{U}=0$ and $\bar{U}=\bar{U}_2$, and we determine the horizontal distance of the two points A and B. For a hyperbolic tangent profile this distance would be 4 times the momentum thickness θ .

We take this artificial momentum thickness θ as our reference quantity. This reference quantity is not too dissimilar to Freymuth's θ_m [17]. Readers who are not satisfied with this crude definition of the momentum thickness θ might redefine it with the data of Figs. 8 and 9.

5. Excitation sound field

The shear layer is excited by two vibrating plates which are driven by electromagnetic loudspeaker systems. In both sets of data (Houston 1981 and Berlin 1983/84) the same vibrating plates had been used. The vibrating plates are operating in antiphase, i.e., both are moving up and down simultaneously and produce a surging flow around the splitter plate edge. The boundary layer suction slit in the splitter plate is not drawn in Fig. 11. During the excitation field measurements, it is sealed anyway. The geometry of our test sections is shown in Fig. 11. To the left hand side of the test sections a nozzle is connected from which the mean flow comes. The region below the symmetry line contains the stream of high velocity \bar{U}_2 . During the excitation field pressure measurements, however, the mean flow is switched off.

Before the data are taken, the pressure probe is moved to the symmetry line $y=0$ at a distance not too close (about $x=10\text{ mm}$) to the edge of the splitter plate. The vibrating plates are

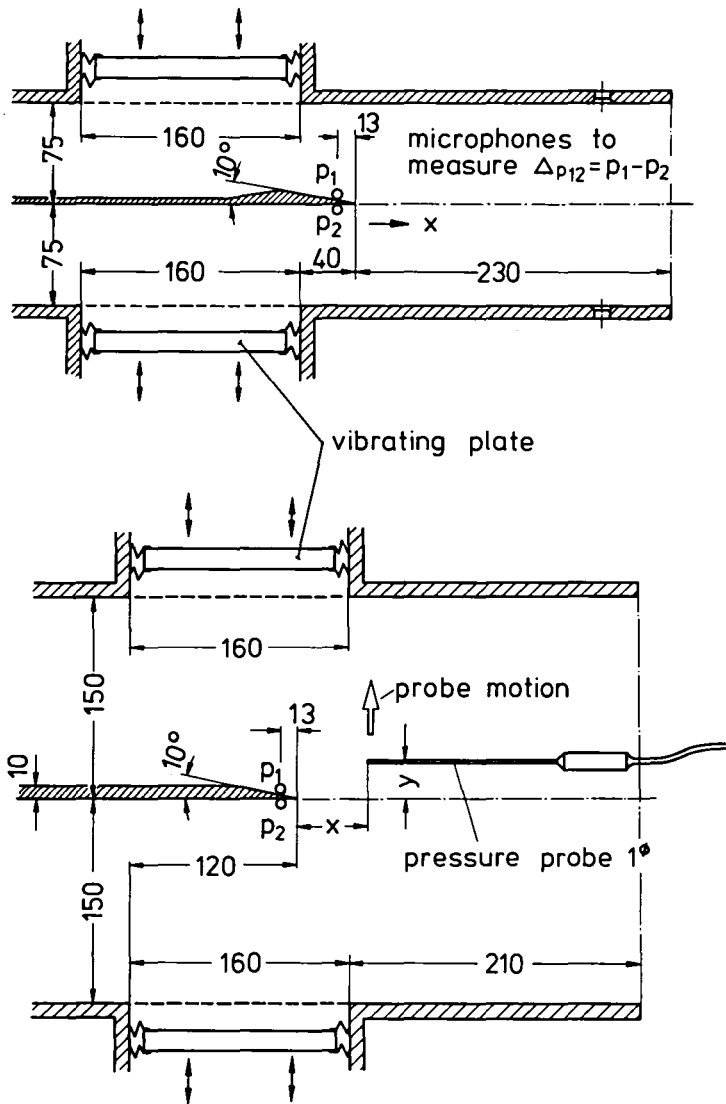


Fig. 11 Configuration of the test sections. Above: Houston 1981, below: Berlin 1983/84.

operated at the frequency of the, later following, shear layer experiment. Then, the phase and magnitude of the vibrating plates is adjusted so that we obtain zero pressure at the probe location.

With this anti-symmetrical adjustment we take the excitation field data. A typical data plot can be seen in Fig. 12. The modulus of the pressure $|p|$ is plotted linearly on the horizontal axis and the vertical distance y from the symmetry line in the test section corresponds to the vertical axis. The phase of p shifts by 180° , if we move the probe from negative y to positive y , so we have indeed an antisymmetric pressure field. Theoretically, the pressures for the various x should all be zero at $y=0$. For the facility is not completely symmetrical, this occurs exactly only at the location where the zero adjustment has been made.

A graphical evaluation of the forcing velocity v_f following the procedure of section 2.2. is shown in Fig. 13. The data of the Houston facility (see Fig. 11) follow exactly the prediction of eq. (4). The vibrating plates of the Berlin facility are located more downstream. This produces a v_f -distribution which follows more the desired $1/\sqrt{x}$ distribution of an "infinite" facility. In the regime, where the shear layer interaction data are taken, up to $x = 30$ mm ($x/d = 0.2$), the Berlin facility shows no deviations from the $1/\sqrt{x}$ law.

For the case with flow, the excitation level Δp_{12} is sometimes not maintained. In particular in the Berlin facility, the excitation field is sometimes slightly changed due to impedance changes of the nozzle with flow. The evaluation of the data is based, however, on a direct measurement of Δp_{12} (with flow) by microphones inserted flush to the side-wall. This requires, that the sound field is strictly two-dimensional, which has been checked carefully. By the way, the proper adjustment of the sound field is not crucial for the shear layer excitation experiments. Nevertheless, it is dependent on an accurate determination of $\Delta p_{12} = \vec{p}_1 - \vec{p}_2$, which is in fact a difference of two vectors. This difference can be taken electronically with two microphones. For

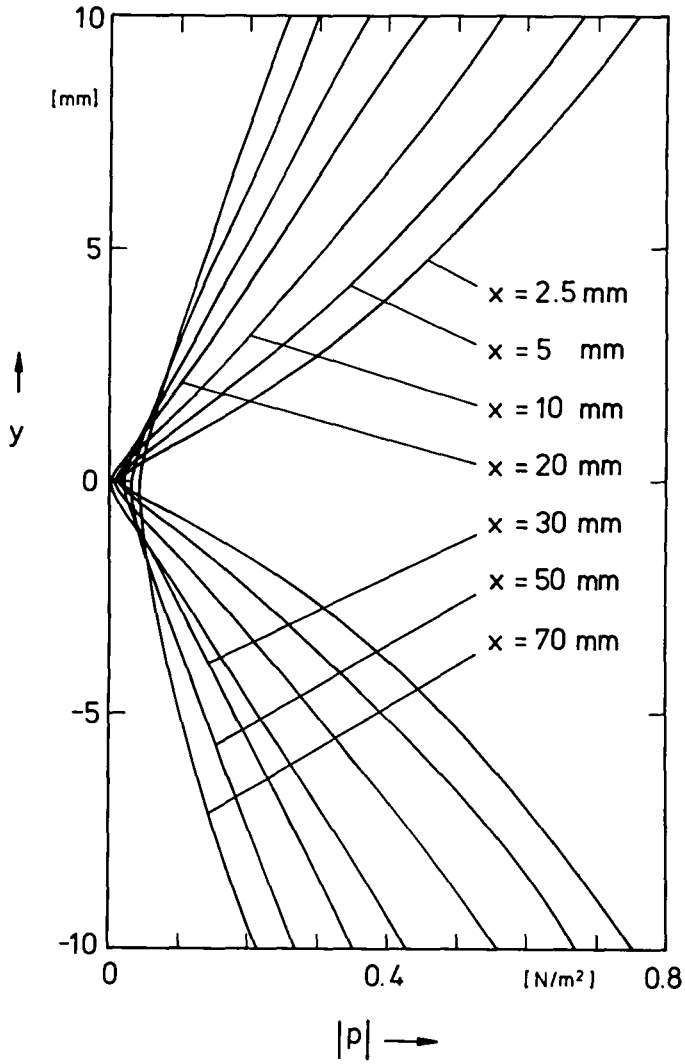
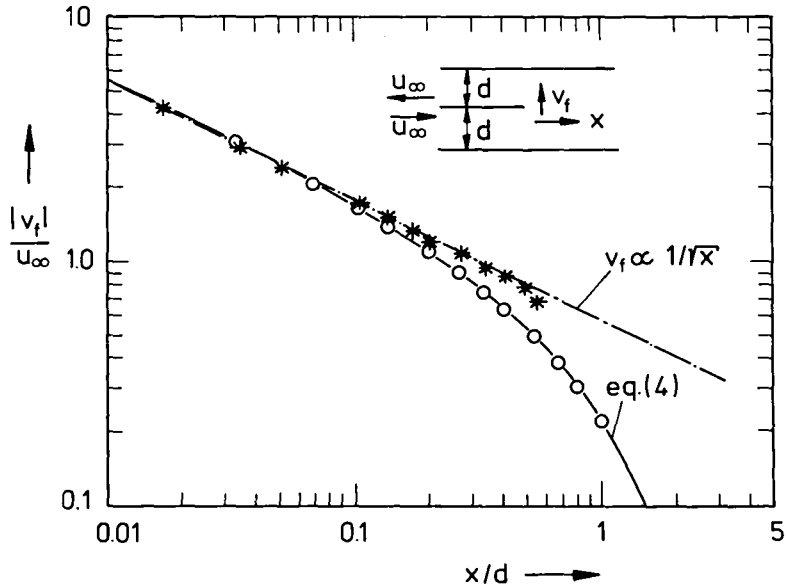


Fig. 12 Fluctuating pressure distribution in the test section without flow. Data taken at $f=200 \text{ Hz}$ in the Berlin facility. x is the distance downstream of the trailing edge of the splitter plate, given in mm.



o	$\hat{=} f = 100 \text{ Hz}$	Houston 1981
x	$\hat{=} f = 100 \text{ Hz}$	} Berlin 1983/84
+	$\hat{=} f = 200 \text{ Hz}$	

Fig. 13 Fluctuating velocity distribution of the forcing field v_f . Comparison between experimental data under different configurations (see Fig. 11) and theory with channel of width $2d$.

better accuracy, however, one microphone is used which is moved from location "1" to location "2". In both locations, magnitude p_1 , p_2 and phase φ_1 , φ_2 relative to an arbitrary reference phase are measured. $|\Delta p_{12}|$ is then determined by vector sub-

traction, namely

$$(23) \quad |\Delta p_{12}| = \sqrt{|p_1|^2 + |p_2|^2 - 2|p_1| \cdot |p_2| \cdot \cos(\varphi_1 - \varphi_2)} .$$

For those who are not acquainted with the logarithmic dB-scale of pressures, we provide here also the conversion from pressure read in dB from sound level meters, to pressures in N/m^2 , as we use them here

$$(24) \quad p[N/m^2] = 2 \cdot 10^{-5} \cdot 10^{(p[dB]/20)} .$$

6. Interaction measurements

6.1. Extrapolated field data

The shear layer is excited at one single frequency. In order to suppress the background noise the velocity signal taken with a hot wire probe is filtered at the same frequency. We will show here data of $|\tilde{u}_2|_{y=0}$, extrapolated from measurements outside the shear layer in the potential flow. We follow the procedure suggested in Fig. 5, section 2.3.. As we have mentioned already, the extrapolation scheme is well suited for a data survey, but it tends to underpredict the velocity values $|\tilde{u}_2|_{y=0}$ for small distances \tilde{x} from the splitter plate edge. In Figs. 14 and 15 we see the data taken in Houston*) and in Berlin. The Houston data show a trend of lower values for small Strouhal numbers which can be explained with a lower excitation due to a narrower test section. The trend is well predicted by our equation (16) in section 2.3.. For higher Strouhal numbers we see a general trend of increasing fluctuation levels well above the theoretical prediction. Significant deviations begin at $S_\theta \approx 0.005$, as expected

*) We should mention, that the data shown in Fig. 14 are the same as those published in [15]. The Strouhal numbers, however, are slightly different. This has two reasons. First, the mean velocity data to determine the momentum thickness θ of the shear layer have been revisited in order to avoid such data where probe interference had changed the measurement of the shear layer profile. Secondly, the momentum thickness θ is now chosen according to the procedure suggested in section 4.

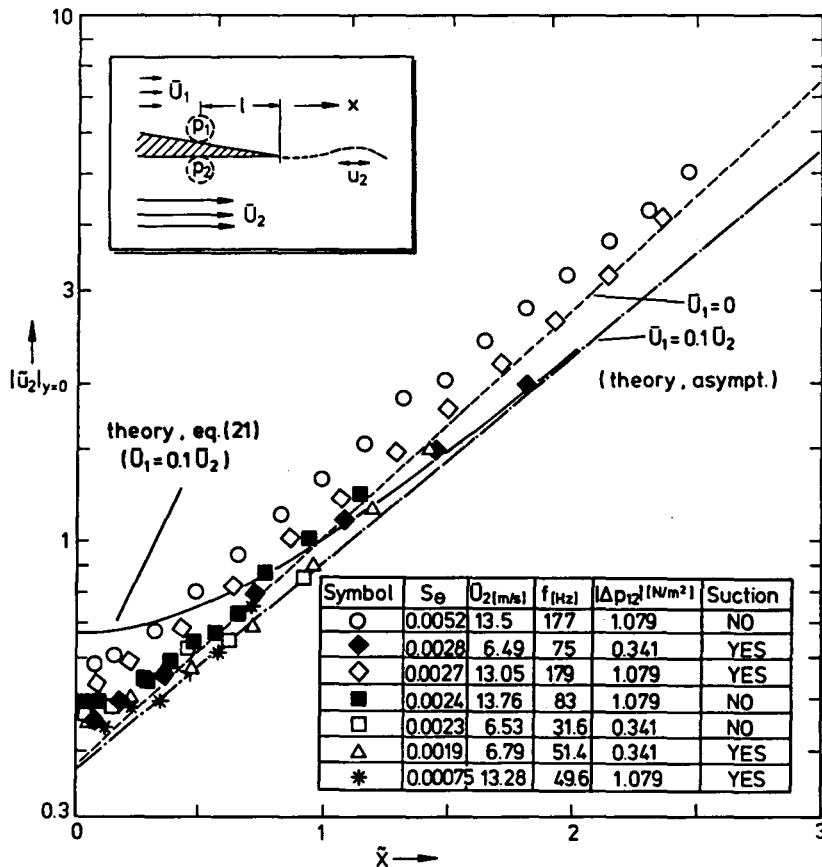


Fig. 14 Shear layer excitation (Data Houston 1981). Experiments with finite shear layer thickness θ versus theory for an infinitesimally thin shear layer. The diagram shows the dependence of the fluctuation velocity $|u_2|_{y=0}$ on the downstream distance \bar{x} for various Strouhal numbers $S_\theta = f\theta/\bar{U}_2$.

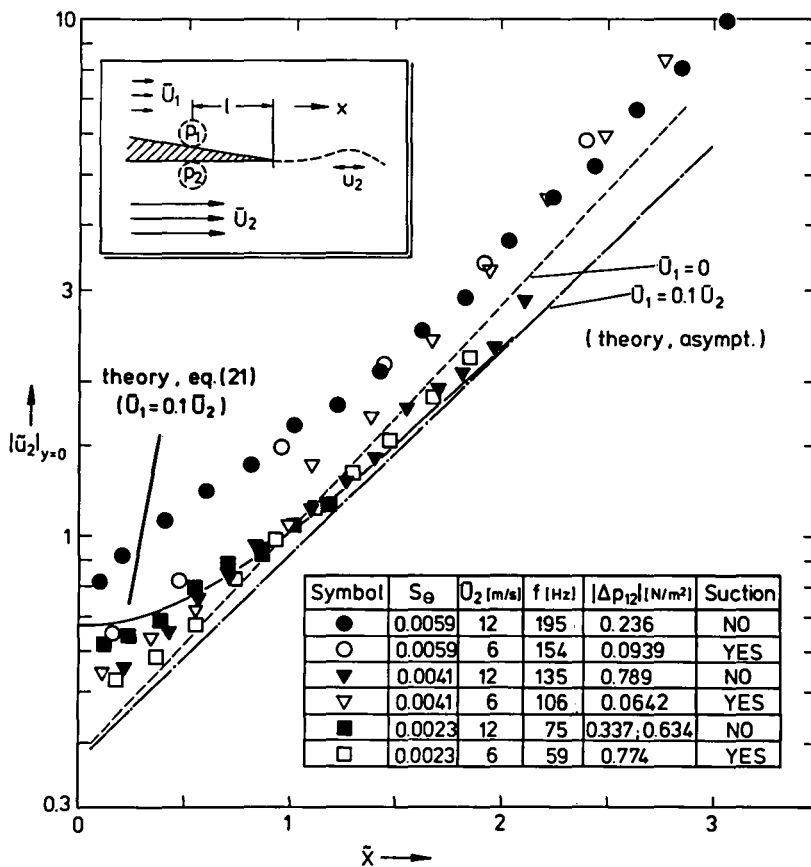


Fig. 15 Shear layer excitation (Data Berlin 1983/84). Experiments with finite shear layer thickness θ versus theory for an infinitesimally thin shear layer. As in Fig. 14, also this diagram shows the dependence of the fluctuation velocity $|\tilde{u}_2|_{y=0}$ on the downstream distance \tilde{x} for various Strouhal numbers S_θ .

in section 2.1. For comparison, we show eq. (21), the theoretical prediction for $\bar{U}_1 = 0.1 \bar{U}_2$, as well as its asymptote for large \bar{x} . We have drawn also the asymptote for $\bar{U}_1 = 0$, the one stream case, i.e., eq. (13) which is the asymptotic form of eq. (15). This comparison shows clearly the influence of the second stream. The real situation, however, is more complex. In the mean flow profiles we see a wake caused by the splitter plate which is filled gradually for increasing downstream distance x (see section 4 on the mean flow field). Therefore, it makes sense to plot both theoretical curves.

6.2. Direct comparison of the field data

For one comparatively low Strouhal number, $S_0 = 0.0023$, we show here measured and computed $|u_2|$ -field data, see Figs. 16 and 17. In the diagrams in each Figure we see a plot of the mean velocity distribution \bar{U} and, with another velocity scale, a (jagged) plot of $|u_2|$. Both are original data from the X-Y-plotter. The quantity y on the horizontal axis is the distance perpendicular from the center of the shear layer. The different diagrams represent different locations upstream and downstream of the edge of the splitter plate. The dotted line represents calculated data of $|\tilde{u}_2|$ from [14] with $\bar{U}_1 = 0$. The symbol "TS" (Two Stream Case) at $y=0$ stands for the analytic solution (eq. (21)) of $|u_2|_{y=0}$. For the case where the second stream with $\bar{U}_1 = 0.1 \bar{U}_2$ is taken into account. For one single downstream location ($\bar{x} = +1$) we have estimated the whole field using the considerations in section 2.4. We see, that the data are well predicted by the theory. In particular, a discrepancy at small and negative \bar{x} , as suggested by the extrapolated data (Figs. 14 and 15), does not exist.

The choice of the origin of y is puzzling at first glance, because $y = 0$, the center of the shear layer, is not identical with the location of the splitter plate wall, as required by the theory. The theory is developed only for an infinitesimally thin shear layer and thus both locations are identical there. However, since there are no infinitesimally thin shear layers in reality, we have to live with this conflict. We observe also, that in cases where the distribution of $|u_2|$ shows a stronger decay in

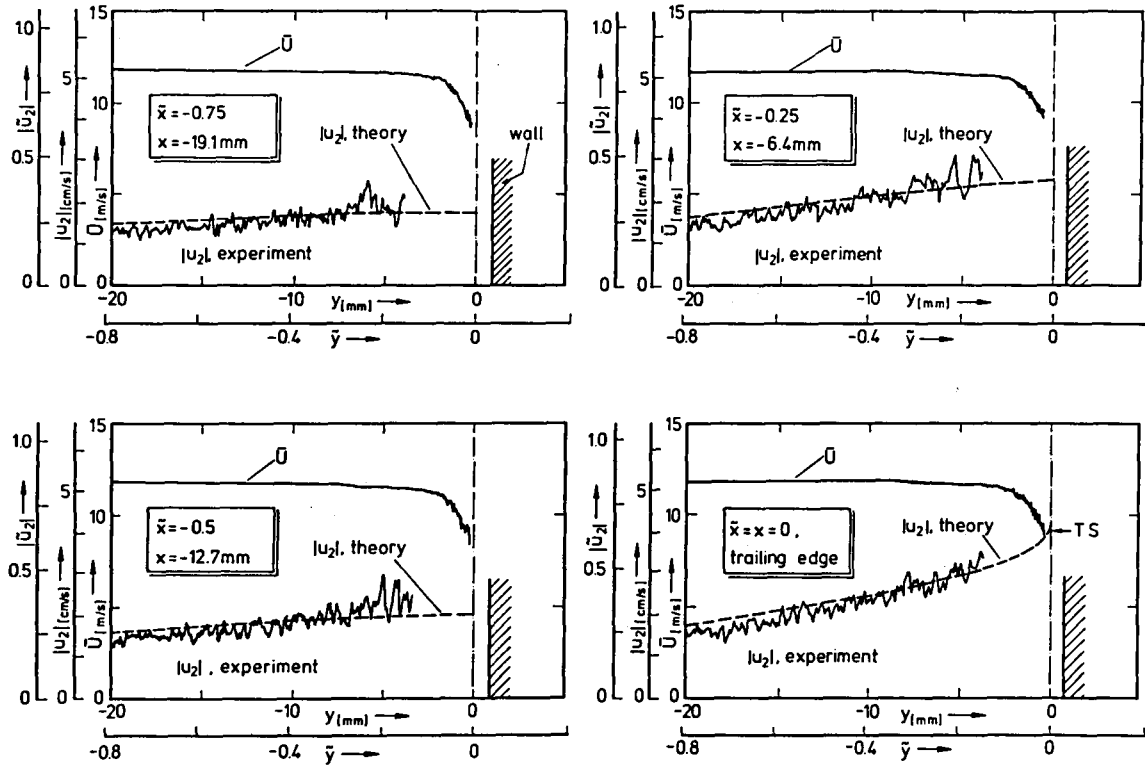


Fig. 16 Velocity fluctuation $|u_2|$ for varying distance y from the shear layer. The plots show measurements upstream of and at the trailing edge. --- = theory for $\bar{U}_1=0$. The experiment is carried out for $\bar{U}_1=0.1 \bar{U}_2$. For this latter case, the analytic solution at $y=0$ is given (TS), eq. (21). Also the mean flow \bar{U} is shown. $S_\theta=0.0023$, $|\Delta p_{12}|=0.634 \text{ N/m}^2$, $\ell=13 \text{ mm}$.

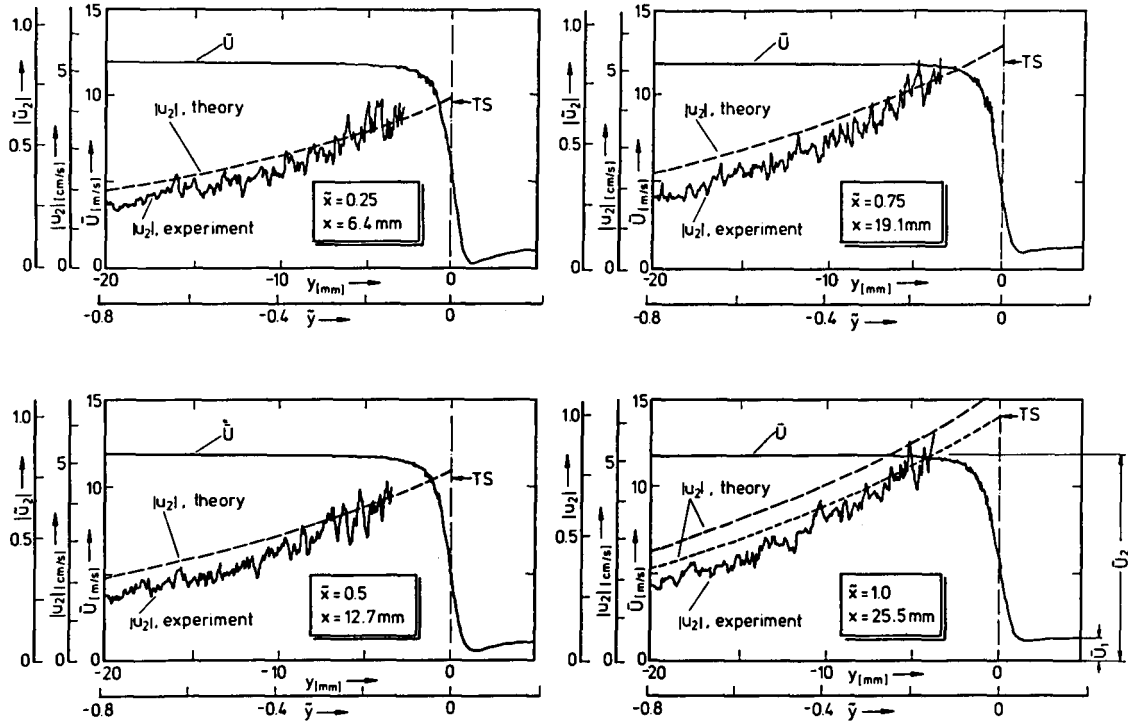


Fig. 17 Velocity fluctuation $|u_2|$ for varying distance y from the shear layer. The diagrams show different locations downstream of the trailing edge. --- = theory for $\bar{U}_1 = 0$. For $\bar{x} = 1$ the theory is also extrapolated to include the second stream $\bar{U}_2 = 0.1 \cdot \bar{U}_1$, "TS" shows the analytic value at $y = 0$, eq. (21). The mean flow is also shown. Other parameters as before.

the -y direction, in particular at high Strouhal numbers, an extrapolation to the "center" of the shear layer can become arbitrary and meaningless. In our data evaluation, this means that the extrapolation scheme breaks down above, say, $S_\theta \approx 0.007$.

The trend, that with increasing Strouhal number the decay of $|u_2|$ in y-direction is enhanced is worth a little further discussion. In a dimensionless representation, however, with $|\tilde{u}_2|$ plotted versus \tilde{y} , this change in the decay rate should be much less dramatic. Nevertheless, if we consider Fig. 2 we see that the real wave number assumes higher values than the theory of an infinitesimally thin shear layer would predict. This produces higher decay rates in the y direction. Our measurements basically confirm this, see Fig. 18.

In Figs. 16, 17 and 18, only the $|\tilde{u}_2|$ -distribution outside the shear layer in the potential flow region was shown. The development of the $|\tilde{u}|$ fluctuations inside the shear layer is shown in Fig. 19. We see the evolution of a steep maximum corresponding to the velocity distribution of the stability calculation of a shear layer with spatial amplification [16]. Upstream of and at the edge of the splitter plate, the fluctuation levels are comparatively low. There is no indication of a singularity at the plate edge which is in agreement with our previous investigations on this issue [18]. As we have mentioned earlier, nonlinearities occur first in locations downstream of the plate edge and inside the shear layer. A direct linearity test for $|u_2|$ can be seen in Fig. 20 in the lower diagram. There, measurements at two different excitation levels are shown. If a doubling of the excitation level produces twice the magnitude of the fluctuation velocities, we can consider the system as linear.

Fig. 20 shows also another important feature of such measurements: there is always contamination by background noise. The typical background noise comes from the flow-producing apparatus, i.e., blower, bends, separation and turbulence in the flow-carrying ducts etc. In particular, low frequency noise below about 100 Hz is very difficult to attenuate by mufflers. In our facilities, we find broad band low frequency noise without pronounced

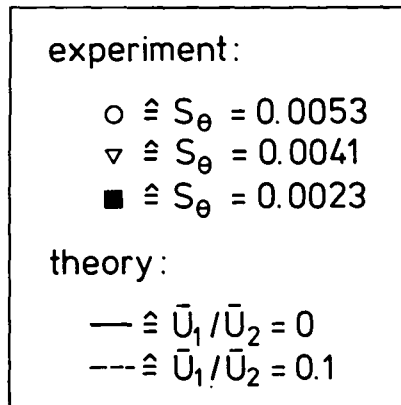
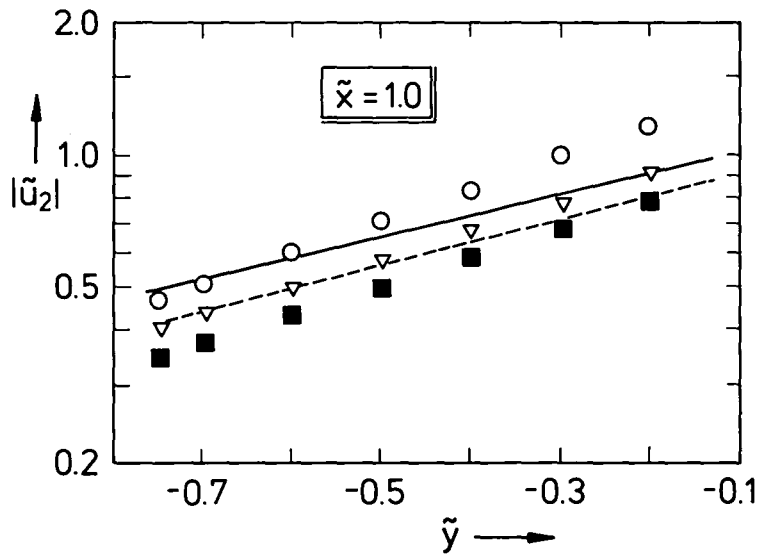


Fig. 18 Decay rate of the velocity fluctuation $|\tilde{u}_2|$ perpendicular to the shear layer at a downstream distance $\tilde{x} = 1.0$. The Strouhal number S_θ is varied.

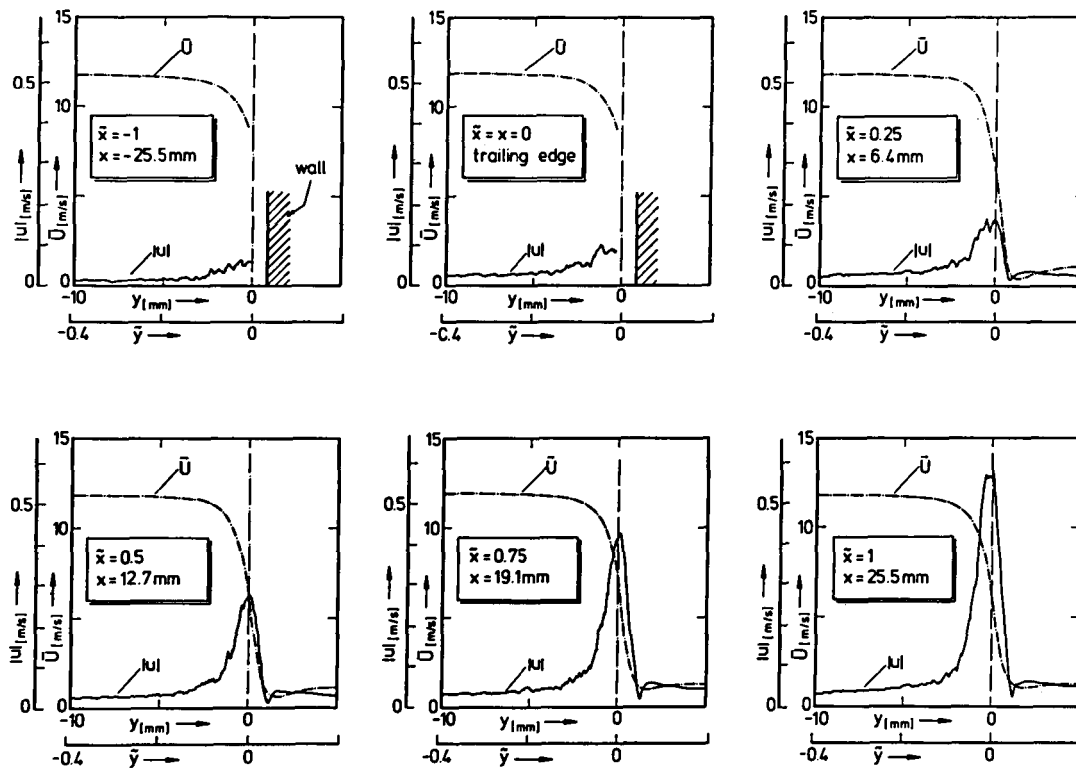


Fig. 19 Velocity fluctuation in the shear layer for varying x . $S_\theta = 0.0023$. Excitation levels as in Figs. 16 and 17.

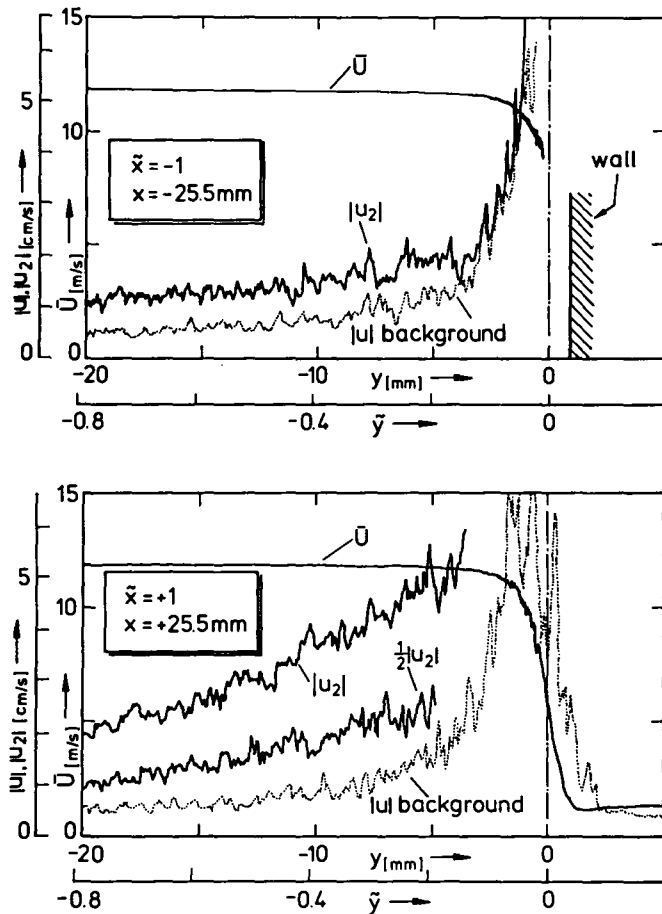


Fig. 20 Background noise in the fluctuation velocity field as compared to the measured signal with tone excitation*). The measurements are taken upstream ($\bar{x}=-1$) and downstream ($\bar{x}=+1$) of the trailing edge of the splitter plate. The plot at $\bar{x}=1$ shows also the linearity of the system by comparing with a fluctuation velocity distribution taken at half the magnitude of the tone excitation. For comparison also the mean velocity distribution \bar{U} is shown. $S_\theta = 0.0023$. Excitation level as in Figs. 16 and 17.

*) The background noise in Fig. 20 is taken with an RMS meter, but the scale is the same as for the sinusoidal signals, i.e., $\sqrt{2}$ times the RMS signal.

peaks in the spectrum. However, also this noise excites the shear layer in the same way as our pure tone excitation does. What we see in Fig. 20, labeled as "background" noise is the narrow band filtered *) signal at the frequency of the excitation, but the excitation is switched off in this case. Uncorrelated background noise begins to become critical for the measurements, if it is more than about 1/2 (= -6 dB) the magnitude of the signal. For - 6 dB background noise contamination, the systematic error becomes 12 %. By the way, this has to be kept in mind also for the measurement of the excitation level, Δp_{12} . These background noise problems cannot be avoided, because increasing the excitation level decreases the possible downstream range of the measurements, because nonlinearities occur earlier. We see from this example, that a low-noise facility, narrow-band filtering and a proper adjustment of the excitation level is very essential for the quality of the measurements.

Finally, it should be mentioned, that the background noise level in Fig. 20 is comparatively high. In fact, it must not be higher than shown there, in order to avoid significant errors. In the other measurements, in general, the background noise contamination is much lower.

6.3. Phase measurements

Phase measurements are most crucial to verify the theory. In these measurements, the phase of u_2 , the fluctuating velocity at $y < 0$, in the mean stream, is measured. The reference phase is that of the vector of the excitation pressure difference $\vec{p}_1 - \vec{p}_2 = \vec{\Delta p}_{12}$. Figs. 21 and 22 show data sets taken at constant distance y from the shear layer. The phase is plotted versus the downstream location x . The data referred to as "theory" had been interpolated from the computed tables given in our previous theory report [14]. The phase angle is counted positive, if there is a phase lag compared to $\vec{\Delta p}_{12}$ (which is the same nomenclature

*) All filtered data are taken with a Brüel & Kjaer 2020 narrow band filter with 3.16 Hz bandwidth. Only the spectra shown in the appendix, section 9.2.5., are taken with a different bandwidth.

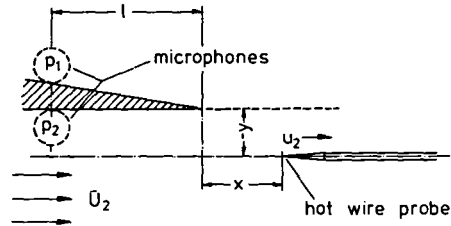
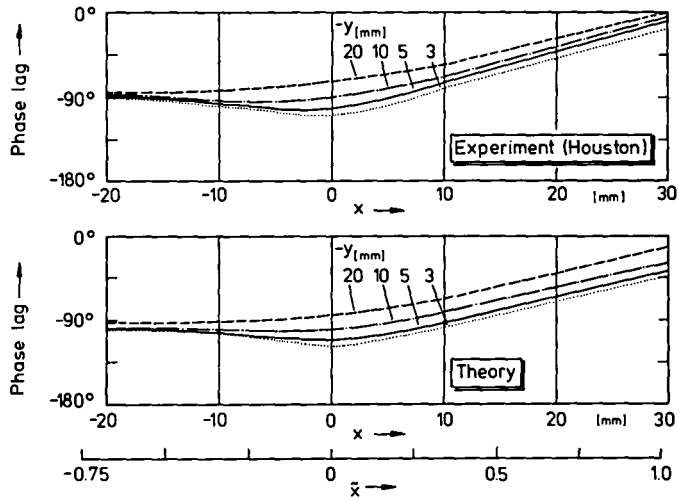


Fig. 21 Phase measurements of the u_2 velocity fluctuations. The reference phase is the phase of the pressure difference $\Delta p_{12} = p_1 - p_2$.

Parameters, dimensional:

$\bar{U}_2 = 13.5$ m/s, $f = 82.5$ Hz, $|\Delta p_{12}| = 0.75$ N/m²; $l = 13$ mm,
 $\theta = 0.395$ mm, without boundary layer suction.

Parameters, nondimensional:

$S_\theta = 0.0024$

$-y$ [mm]	3	5	10	20
$-\bar{y}$	0.115	0.192	0.384	0.768

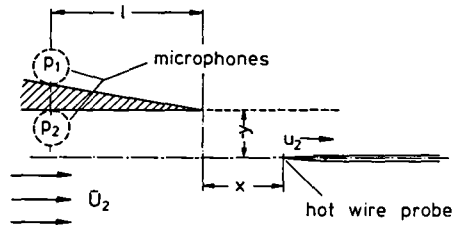
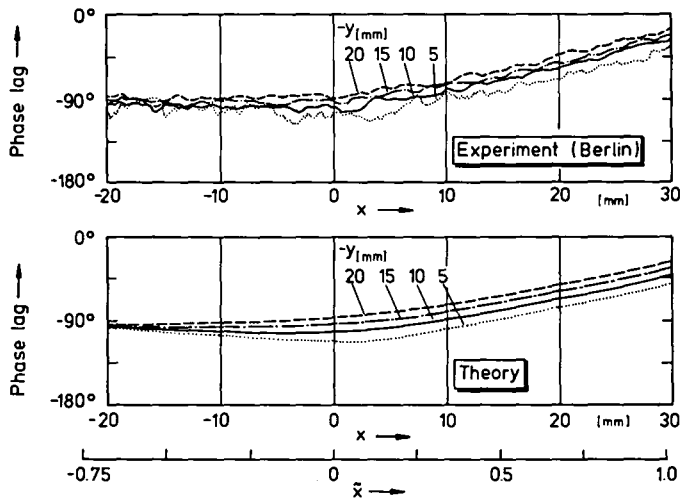


Fig. 22 Phase measurements of the u_2 velocity fluctuations. The reference phase is the phase of the pressure difference $\Delta p_{12} = p_1 - p_2$.

Parameters, dimensional:

$\bar{U}_2 = 12$ m/s; $f = 65$ Hz; $|\Delta p_{12}| = 0.75$ N/m²; $l = 13$ mm.

$\theta = 0.225$ mm; with boundary layer suction.

Parameters, nondimensional:

$S_\theta = 0.00122$

$-y$ [mm]	5	10	15	20
$-\tilde{y}$	0.17	0.34	0.51	0.68

as in the tables [14]). The data have been taken in two different facilities (Houston and Berlin) and at two different Strouhal numbers S_0 . The Berlin data show more jitter due to background noise. The agreement, however, is remarkable. We see only minor discrepancies farther downstream, caused by a slightly lower phase speed than anticipated by the "thin shear layer" theory. This comes not unexpected for a shear layer of finite thickness (see Fig. 2). Near the trailing edge, there is a local region of negative phase speed *) , as predicted by the theory. This does not indicate negative group speed or any feedback from downstream locations, it is a side effect in the potential field around an excited shear layer.

The general trend of the measurements is quite simple: for negative x , upstream of the edge, we find the phase of the excitation field, which is dominating there. For regions of positive x , farther downstream of the edge, the instability wave dominates, with a phase speed close to the mean flow speed \bar{U}_2 . The planes of equal phase are inclined for spatial stability waves. Therefore, we have different phases for different y at constant downstream location x .

6.4. Measurements at higher Strouhal numbers

For higher Strouhal numbers we cannot compare the experimental data with a detailed theory, but some simple considerations provide an understanding of the measurements. The data which we show are taken at $S_0 = 0.0136$, close to the frequency where maximum amplification occurs (see Fig. 2). First, we show some fluctuation magnitude measurements, Fig. 23. We see, that the decay of $|u|$ in the y direction is so rapid, that the decay takes place essentially within the shear layer. The velocities outside the

*) We have found such local regions of negative phase speed already in previous experiments [18, 19] also inside the shear layer. There, the location where the phase measurements were taken, was the local $|u|$ maximum location which shifts in its y position for small distances x from the trailing edge. So the conclusion of having found negative phase speeds had then still some ambiguity in it. For regions farther downstream, however, where the shear layer has developed, the procedure cannot be criticized.

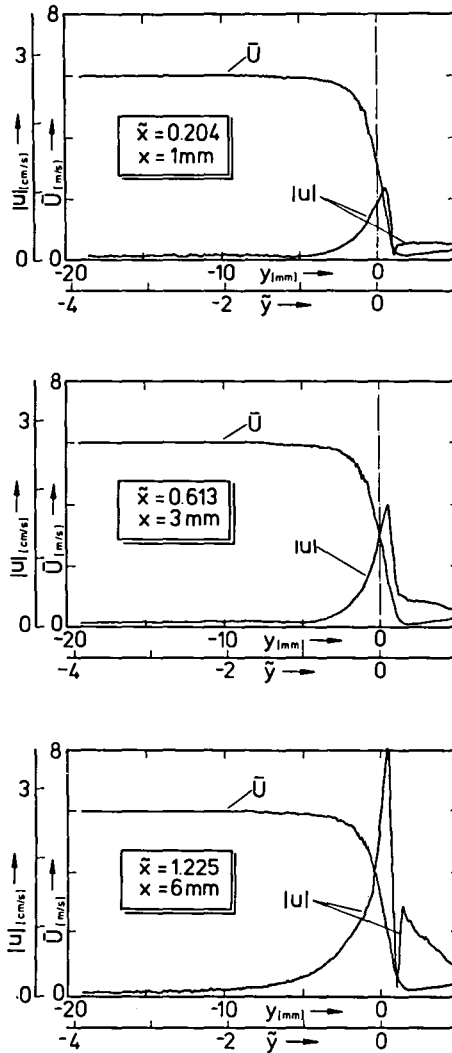


Fig. 23 Distribution of the $|u|$ velocity fluctuations at higher Strouhal number $S_\theta = 0.0136$, close to the condition of maximum spatial amplification. Excitation pressure difference $\Delta p_{12} = 0.103 \text{ N/m}^2$, $l = 13 \text{ mm}$, no boundary layer suction.

shear layer are produced essentially by the excitation field, which has very low induced $|u|$ -levels close to the shear layer. So we find, in particular at small x , a very low $|u|$ -level close to the shear layer, which looks almost like a local node.

In Fig. 24 we see phase measurements at the same Strouhal number. The general trend is the same as at lower Strouhal numbers: We have the excitation field and its phase dominating at negative x , upstream of the trailing edge. Far downstream, say, at $x > 25$ mm in our diagram, the instability wave with its tilted wave fronts dominates. The intermediate region looks more puzzling, but is easy to explain. We know that the instability wave influence decays exponentially for increasing y . So the x location where the instability wave takes over is different for different y . At $y = -5$ mm, e.g., the instability wave takes over just at the trailing edge. For greater distances y , this transition point shifts more towards the downstream direction. The superposition of these two fields produces locally regions of negative phase speed. If we want to extrapolate this trend to even higher Strouhal numbers, we will find a very detailed local structure like the one Pfizenmaier [20] found in a jet at very high Strouhal numbers. But we have to stress this again: the local occurrence of negative phase speeds in our experiments is a consequence of the interaction of propagating shear layer waves and (essentially) standing sound waves. It does not allow the conclusion that these regions are produced by sources located downstream. This is only a warning; we do not deny effects from downstream in general. A discussion on downstream effects, and the conclusion that they are probably weak, is given in [14].

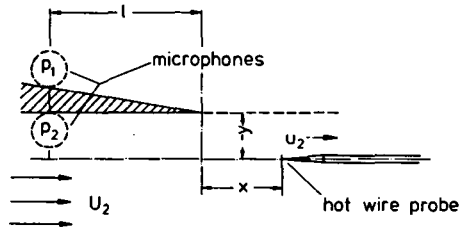
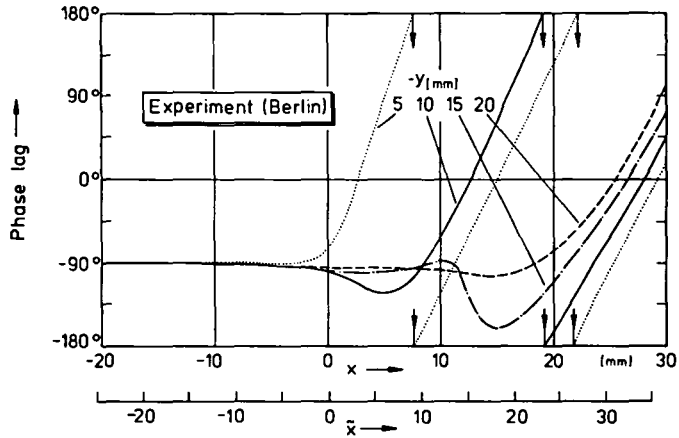


Fig. 24 Phase measurements of the u_2 velocity fluctuations. The reference phase is the phase of the pressure difference

$$\Delta p_{12} = p_1 - p_2.$$

Parameters, dimensional:

$$\bar{U}_2 = 6 \text{ m/s}; f = 195 \text{ Hz}; |\Delta p_{12}| = 0.103 \text{ N/m}^2; \ell = 13 \text{ mm};$$

$\theta = 0.42 \text{ mm}$, without boundary layer suction.

Parameters, nondimensional:

$$S_\theta = 0.0136$$

$-y$ [mm]	5	10	15	20
$-\bar{y}$	4.08	8.16	12.24	16.32

7. Conclusions

We have carried out hot wire and microphone measurements to check our previous theory of the acoustical excitation of shear layers [14]. This theory suggested that the fluctuation field can be split into two constituents:

- (a) the excitation pressure field which is transmitted through the shear layer, and
- (b) the pressure field which, as a reaction, is produced by the shear layer itself.

The excitation (a) generates an antisymmetrical field close to the splitter plate edge. Therefore, it produces a pressure difference ($|\Delta p_{12}|$) on both sides of the splitter plate. On the other hand, the field induced by the shear layer (b) is symmetrical with respect to the shear layer; hence it does not contribute to the pressure difference $|\Delta p_{12}|$ on both sides of the splitter plate. Consequently, the pressure difference Δp_{12} is the relevant quantity for the acoustical excitation.*) In addition, our previous theory provides numerical data for velocity fluctuation levels and phase angles in the flow field near the plate edge. Moreover, this theory does not contain any empirical constants.

The experiments have been carried out in two similar facilities (Houston 1981 and Berlin 1983/84). The measurements were conducted with a shear layer in the center of a channel having a rectangular cross section and with air as a fluid. The acoustical excitation was provided by two vibrating plates, which produced a surging motion around the splitter plate edge, from which the shear layer was shed. The shear layer was initially laminar and its thickness could be controlled by boundary layer suction. The data were taken in the vicinity of the trailing edge of the

*) Note that $|\Delta p_{12}| = |\vec{\Delta p}_{12}| = |\vec{p}_1 - \vec{p}_2|$ is a difference of two vectors, i.e., of two pressures with different modulus and phase. This means that either $|\Delta p_{12}|$ is measured directly with two microphones or calculated after an independent measurement of the two pressures and their phases, using eq. (23) in section 5.

splitter plate. There, all fluctuating quantities were small and a comparison with the above mentioned linear theory appeared to be meaningful. In addition, the measurements were concentrated on comparatively low Strouhal numbers where a comparison with the theory for a "thin" shear layer [14] makes sense. Also the so-called large scale structures in a shear layer correspond to low Strouhal numbers. Therefore, the present investigation may provide some solid background information on how these structures can be generated or enhanced. However, we do not show any own flow visualization pictures here, because the interaction region near the trailing edge exhibits comparatively low fluctuation levels and hence flow visualization would show an apparently undisturbed laminar flow there.

The present measurements are based on:

- (i) a determination of the magnitude of excitation by microphone measurements of the pressure difference Δp_{12} on both sides of the splitter plate, and
- (ii) hot wire measurements of the u-fluctuation levels and their phase in the region of the mean flow below the shear layer.

The latter hot wire measurements are compared with computed theoretical values [14]. The agreement between theory and experiment is very encouraging, in particular in the validity range of "thin" shear layer theory, i.e., for Strouhal numbers $S \leq 0.005$ *). The measurements show even minor details that were predicted by the theory, such as local regions of negative phase speeds of the u-fluctuations. However, these regions of negative phase speeds have nothing to do with upstream effects of sound sources located downstream in the turbulent shear layer. They are nothing else but an accurately predicted side effect of the

*) The Strouhal number appears to be comparatively low. This is due to the definition of S_0 which is calculated with a small quantity, i.e., the momentum thickness, which is much smaller than other typical dimensions of the shear layer. In that context, it is worth mentioning, that the whole range of amplified instability waves of a shear layer is in the range $0 < S_0 < 0.04$.

shear layer excitation.

Finally, it should be mentioned, that we have now experimental proof of the existence of a Kutta condition for the fluctuating flow of an excited shear layer shed from a trailing edge. The statement is valid for low Strouhal numbers at least up to $S_0 = 0.005$. This can be concluded from the fact that the measured velocity and phase distributions fit very well the theoretical values calculated for this condition. It supports also the theoretical proof of the same issue, given in our previous investigations [14].

The theory which is now shown to be valid predicts the fluctuating potential flow field outside the shear layer. A prediction of the fluctuations inside the shear layer is also possible, at least downstream of the interaction region at the edge. This can be done by adjusting the potential field of our "thin" shear layer theory to the calculated potential field for a shear layer with finite thickness, but infinitely extended in the streamwise direction [16]. Thus, the complete perturbation input of a shear layer exposed to a sound field can be predicted. Of course, this statement is only valid for low Strouhal numbers, $S_0 \leq 0.005$, but it may be also useful for estimations at higher Strouhal numbers.

Acknowledgement

The present work has been sponsored partly by NASA Lewis (Contract NAG 3-198) and by the Deutsche Forschungsgemeinschaft (Contract Be 889/1-1). Most of the equipment used in Berlin comes from earlier DFG contracts, e.g., the vibration systems (Wi 8/35) and the blower as well as the probe traverse hardware (Wi 8/37). The improved electronic instrumentation of the probe traverse was prepared by B. Simon.

The authors were encouraged by Professor A.K.M.F. Hussain (University of Houston) to carry out this research. He helped also to arrange for one of the author's (D.W.B.) visit as an associate professor to Houston in this joint U.H.-DFVLR project.

8. References

- [1] Leconte, J. On the influence of musical sounds on the flame of a jet of coal-gas. The London, Edinburgh, and Dublin Philosophical Magazine and Journal of Science 15 (1858), pp. 235-239.
- [2] Tyndall, J. Sound. London: Longmans, 1867.
- [3] Michel, F. Lärm und Resonanzschwingungen im Kraftwerksbetrieb. (Noise and resonant vibrations in power plants.) Berlin: VDI-Verlag, 1932. The authors owe this reference to Dr. A. Dinkelacker, who found this book in L. Prandtl's private library.
- [4] Crow, S.C. Champagne, F.H. Orderly structure in jet turbulence. J. Fluid Mech. 48 (1971), pp. 547-591.
- [5] Dziomba, B. Experimentelle Untersuchung zum Einfluß von Anfangs- und Randbedingungen auf die Ausbreitung einer freien zweidimensionalen Scherschicht. Dissertation, Techn. Univ. Berlin, Fachbereich 9, 1981.
- [6] Gutmark, E. Ho, C.-M. Preferred modes and the spreading rates of jets. Phys. Fluids 26 (10), October 1983, pp. 2932-2938.
- [7] Bechert, D.W. Pfizenmaier, E. On the amplification of broad band jet noise by a pure tone excitation. J. Sound and Vibr. 43 (1975), pp. 581-587.
- [8] Moore, C.J. The role of shear-layer instability waves in jet exhaust noise. J. Fluid Mech. 80 (1977), pp. 321-367.
- [9] Deneuille, P. Jaques, J. Jet noise amplification: a practically important problem. AIAA 4th Aeroacoustics Conference, Oct. 3 -5 , 1977, Atlanta/Ga., AIAA paper 77-1368.

- [10] Crighton, D.G.
Leppington, F.G. Radiation properties of the semi-infinite vortex sheet: the initial value problem.
J. Fluid Mech. 64 (1974), pp. 393-414.
- [11] Bechert, D.W.
Michel, U. The control of a thin free shear layer with and without a semi-infinite plate by a pulsating flow field.
ACUSTICA 33 (1975), pp. 287-307.
- [12] Möhring, W. On flows with vortex sheets and solid plates.
J. Sound & Vibr. 38 (1975), pp. 403-412.
- [13] Rienstra, S.W. Edge influence on the response of shear layers to acoustic forcing.
Ph. D. Thesis, Univ. Eindhoven, Netherlands, June 1979.
- [14] Bechert, D.W. Excited waves in shear layers.
DFVLR-FB 82-23 (1982).
- [15] Bechert, D.W. A model of the excitation of large scale fluctuations in a shear layer.
AIAA 8th Aeroacoustics conference, April 11 -13 , 1983, Atlanta/Ga., AIAA paper 83-0724.
- [16] Michalke, A. On spatially growing disturbances in an inviscid shear layer.
J. Fluid Mech. 23 (1965), pp. 521-544.
- [17] Freymuth, P. On transition in a separated laminar boundary layer.
J. Fluid Mech. 25 (1966), pp. 683-703.
- [18] Bechert, D.W.
Pffizenmaier, E. Optical compensation measurements on the unsteady exit condition at a nozzle discharge edge.
J. Fluid Mech. 71 (1975), pp. 123-144.
- [19] Bechert, D.W.
Pffizenmaier, E. On wavelike perturbations in a free jet travelling faster than the mean flow in the jet.
J. Fluid Mech. 72 (1975), pp. 341-352.

- [20] Pfizenmaier, E. Zur Instabilität des schallbeeinflußten Freistrahls.
DLR-FB 73-69 (1973).
Available in English:
On the instability of a sound-influenced free jet.
ESRO TT 122 (1973).
- [21] Bechert, D.W. Die Steuerung eines ebenen turbulenten Freistrahls durch eine seitliche Wechselströmung, erzeugt in einem Schallfeld.
(The control of a plane turbulent jet by a perpendicular fluctuating flow generated in a sound field.)
Z. Flugwiss. 24 (1976) 1, pp. 25-33.
- [22] Bechert, D.W. Versuchseinrichtungen zur Untersuchung der Steuerung eines ebenen Freistrahls durch Schall.
(Facility to investigate the control of a plane jet by sound.)
Bericht: Hermann-Föttinger-Institut für Strömungstechnik, TU Berlin, Juni 1966.
- [23] Beranek, L.L. Acoustic Measurements.
New York: J. Wiley & Sons, 1965.

9. Appendices

9.1. Appendix A

Glossary of Symbols

d	half width of the two-dimensional channel of the test section
dB	logarithmic unit for the fluctuating pressure, the relation to linear units is given by eq. (24)
dBA	"A-weighted" fluctuating pressure. This unit was established to simulate the frequency dependence of the sensitivity of the human ear. Thus, very low frequencies, say, below 200 Hz do not enter in the dBA level significantly. For details see textbooks in acoustics, e.g., [23], p. 892
erf(z)	<u>error function</u> , defined as $\text{erf}(z) = \frac{2}{\sqrt{\pi}} \int_0^z e^{-s^2} ds$
f	<u>frequency</u> of the excitation $f = \omega/2\pi$
i	<u>imaginary unit</u> $i = \sqrt{-1}$
l	distance between the edge of the splitter plate and the pressure pickup devices, i.e., the microphones, at both sides of the plate
p	pressure. The fluctuating pressure, i.e., the deviation from the ambient atmospheric pressure. All perturbation quantities are proportional to $e^{-i\omega t}$
p ₀	reference pressure of the pressure fluctuations: $p_0 = 2 \cdot 10^{-3} \text{ N/m}^2$
p ₁	fluctuating pressure above the splitter plate (see Fig. 3)
p ₂	fluctuating pressure below the splitter plate (see Fig. 3)
Δp_{12}	pressure difference $\Delta p_{12} = p_1 - p_2$. Note that this is a <u>vector difference</u> , so the phases of p ₁ and p ₂ have to be taken into account. (see eq. (23) in section 5)
p _s	fluctuating pressure in the <u>settling chamber</u>
t	time
u	fluctuating velocity component in the x-direction. All fluctuating quantities are proportional to $e^{-i\omega t}$
u ₁	fluctuating u velocity component above the shear layer at $y > 0$

u_2 fluctuating u velocity component below the shear layer at $y < 0$

u_{ref} reference velocity, defined by eq. (10) as

$$u_{ref} = \frac{|\Delta p_{12}|}{\rho \sqrt{U_2} \omega \ell}$$

u_∞ fluctuating velocity at large negative x in a channel with a splitter plate where the sound sources are assumed to be located at $x = -\infty$. This quantity is related to the pressures at the splitter plate by eq. (3)

$$u_\infty = \frac{|\Delta p_{12}|}{\rho \omega \sqrt{\ell}} \cdot \sqrt{\pi/d}$$

\tilde{u} dimensionless fluctuating velocity in x direction,
 $\tilde{u} = u/u_{ref}$

$|\tilde{u}_2|$ Peak value modulus of the dimensionless velocity \tilde{u}_2 , the index "2" labels the region below the splitter plate, $y < 0$.

v fluctuating velocity component in the y direction. All fluctuating quantities are proportional to $e^{-i\omega t}$

v_f fluctuating v velocity of the acoustic forcing field

v_1 fluctuating v velocity above the shear layer for $y > 0$. In equations (6), (8), (9), (11) and (13) we mean the velocity just above the shear layer v_1 $y=+0$

\tilde{v}_1 dimensionless v velocity above the shear layer, defined as $\tilde{v}_1 = v_1/u_{ref}$

x horizontal coordinate in direction of the mean flow

\tilde{x} dimensionless horizontal coordinate, defined as $\tilde{x} = x\omega/\bar{U}_2$

y vertical coordinate

\tilde{y} dimensionless vertical coordinate, defined as $\tilde{y} = y\omega/\bar{U}_2$

C Coefficient, decreasing the value of the shear layer fluctuations due to the influence of the channel walls of the test section. C is defined by eq. (16)

L, L_2, L_s, L_{12} filtered background noise pressure in dB/Hz, taken in different locations, see Figs. 38-40

S_θ Strouhal number calculated with the momentum thickness θ of the shear layer and defined as $S_\theta = f \cdot \theta / \bar{U}_2$

"TS"	TS refers to the two stream case and indicates in the diagrams, where it is used, the value of the velocity $ \tilde{u}_y $ just below the shear layer at $y = -o$. In this calculated value, the low speed \bar{U}_1 of the second stream above the shear layer is taken into account.
\bar{U}	mean flow velocity in x direction
\bar{U}_1	mean flow velocity above the shear layer for $y > o$
\bar{U}_2	mean flow velocity below the shear layer for $y < o$. \bar{U}_2 is much greater than \bar{U}_1 .
α_i	imaginary part of the complex wave number α of an instability wave ($i\alpha = \lambda$)
α_r	real part of the same complex wave number
λ_i	imaginary part of the complex wave number of the instability wave in a shear layer
λ_r	real part of the complex wave number of the instability wave in a shear layer
$\lambda_{1,2}$	complex wave number of the instability wave in a shear layer $\lambda_1 = \frac{\omega}{\bar{U}_2} (i+1) ; \quad \lambda_2 = \frac{\omega}{\bar{U}_2} (i-1)$
$\tilde{\lambda}_{1,2}$	dimensionless wave number of the instability wave, see eq. (19)
ρ	density of the fluid, in our experiments air at room temperature
σ	velocity ratio of the two streams above (\bar{U}_1) and below (\bar{U}_2) the shear layer. $\sigma = \bar{U}_1/\bar{U}_2$
φ_1, φ_2	phase angles of the pressure p_1 and p_2 , respectively. The reference phase may be arbitrary, e.g., the phase of the beat frequency oscillator which drives the excitation sound field
ω	radian frequency of the excitation sound field $\omega = 2\pi f$
θ	momentum thickness of the shear layer, for definition see Fig. 10 in section 4.
Indices:	The index "1" denotes quantities above the shear layer ($y > o$).
	The index "2" denotes quantities below the shear layer ($y < o$).
	The tilde "~" denotes dimensionless quantities.

The quantities between vertical bars, e.g., $|u_2|$ refer to the peak value of these quantities in a sinusoidal vibration.

The dB or dBA readings of broad band signals in the appendix, section 9.2.5. refer to the RMS value of these signals.

The background noise in Fig. 20 was taken with an RMS meter, but the scale is the same as for the sinusoidal signals, i.e., $\sqrt{2}$ times the RMS signal is given there.

9.2. Appendix B: Experimental apparatus

9.2.1. Facility Houston

Fig. 25 shows a sketch of the facility which had been established in 1981 at the University of Houston. The air supply consists of a centrifugal fan having backward curved blades in a cast aluminum impeller and with a casing of high aerodynamic quality ("American Standard"), driven by a D.C. motor with variable shaft speed. In addition, the fan has a comparatively low noise output. The fan-motor unit has a separate suspension to prevent vibrations from being transmitted to the facility. The fan is connected by an elastic hose and with a little diffuser to two commercial broad band mufflers. To the other side of the mufflers a long diffuser is connected. This diffuser contains 3 regular screens to keep the flow attached. A little settling chamber is connected to the diffuser, which produces also a merging from circular to quadratic cross section. A nozzle follows with two ultra-fine screens (200 x 200 mesh x 0.0021" diameter, stainless steel wire cloth, equivalent to 8 wires per mm, each wire 0.053 mm in diameter) at its entrance section. This nozzle is connected to the high-speed side of the test section. The exact dimensions of the test section are given in Fig. 11 in section 5. The height of the test section channel is 100 mm and the maximum mean flow velocity is 17 m/s. The second stream is merely driven by the entrainment of the shear layer. Its velocity is about one tenth of the mean stream velocity. There is some turbulence generated by local separations in the duct of the second stream. However, this does not seem to have a perceivable influence on the measurements.

The whole structure is mounted on saw-horses on a wooden frame in an anechoic chamber (see Fig. 26). In principle, it is not necessary to use an anechoic chamber for such an experiment, but usually it is the room with the lowest background noise in a laboratory. Also, the noise from fan, suction blower and cooling fans from the electronic instrumentation propagates and decays with distance like in open air and thus, if the spatial distance is a few meters from the test section, this does not affect the

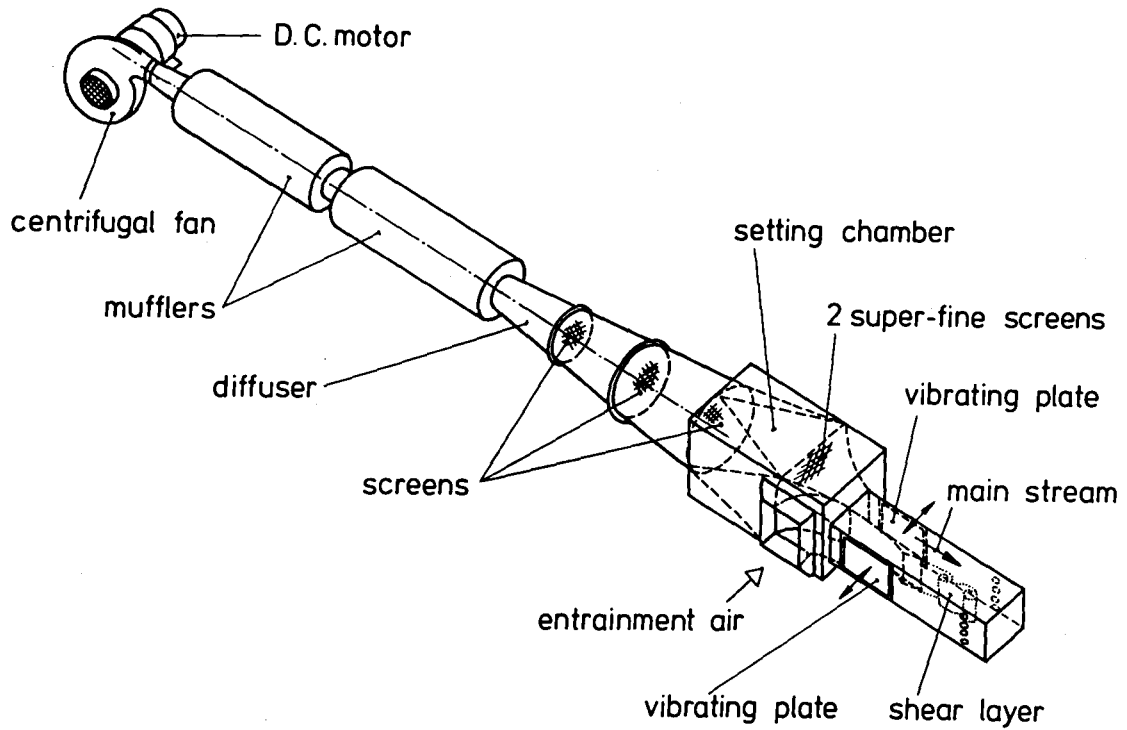


Fig. 25 Schematic view of the facility at the University of Houston.

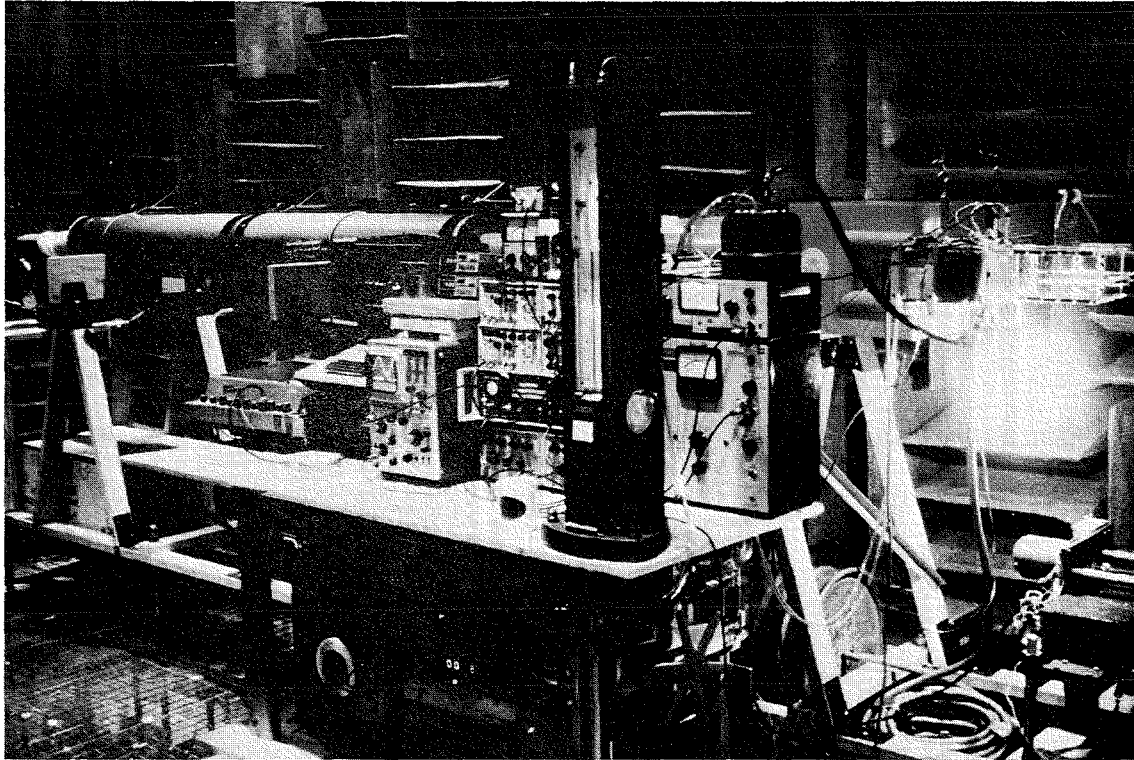


Fig. 26 Side view of the facility at the University of Houston, installed in the anechoic chamber of the Department of Engineering.

measurements.

This facility as well as the one we used in Berlin are very quiet indeed. At operational air speed ($\bar{U}_2 = 12$ m/s) the facility is almost inaudible, the dominant noise sources (for the ear) are the flow separations from the probe supports immersed into the main stream. The authors claim that they have never seen (or better: heard) such silent shear layer or jet facilities except the facility which had been used by Wehrmann, Michalke and Freymuth [17].

To move the pressure and velocity probes in the test section a mini-computer controlled traverse with stepper motors is used. The traversing speed can be changed by the computer software. The traverse is used in continuous motion during the continuous plots on an X-Y-plotter. This admitted abuse of the traverse is difficult to carry out, because the stepper motors cause significant vibration of the probes. To suppress these vibrations an inertia mass with an elastic link is used between stepper motor and the driving screw of the traverse, which moves the probes. The benefit of this continuous data recording is a very rapid data acquisition. It produces curves which show even minor subtleties of the measurements at once. In addition, the complete data acquisition could be disconnected from the (overloaded, time sharing) central process computer of the U.H. turbulence laboratory which again accelerated the experiments by one order of magnitude. The instrumentation is partly visible in Fig. 26. Because it is very similar to the instrumentation of our Berlin facility, it is not discussed here in detail.

9.2.2. Facility Berlin

In Fig. 27 a sketch of the Berlin facility can be seen. Some parts are omitted, e.g., the air supply unit. We use again a centrifugal fan with backward curved blades which is driven by a D.C. motor with variable speed. The shaft speed is controlled by a digital control unit, built by our electronics shop (DFVLR DMR II). To suppress noise we use a muffler. The settling chamber (see Fig. 27) is also used as a muffler by a glass fiber filling. A double nozzle is attached to the settling chamber. Be-

tween settling chamber and nozzle we use again an ultra-fine screen on the side of the main stream (left in Fig. 27). The low speed on the right hand side is produced by a high flow resistance with foam, a ultra-fine screen and perforated metal sheet. Here, we use a very fine metal sheet with holes which are hardly visible to the naked eye (9 circular holes per mm², hole diameter 0.3 mm). The same material is used to cover the "windows" to which the vibration systems are attached at the sides of the test section (see Fig. 28).

The boundary layer control bleeding holes (see Fig. 27) are the solution of a serious problem in this type of facility. Without these holes, the boundary layer distribution is not even in the vertical direction on the splitter plate. In particular, in the center of the splitter plate, the boundary layer exhibits a bulge in the distribution, very different from the expected Blasius velocity profile. After a long series of tests, this deficiency could not be attributed anymore, as argued initially, to perturbations caused upstream of the nozzle. In fact, this deficiency is due to a secondary flow, from the corners to the center line, inside the nozzle. The bleeding holes provide a pressure distribution inside the nozzle, which eliminates this secondary flow and with it the bulge in the mean velocity profile. In the sketch in Fig. 27 it is not indicated that the bleeding holes are covered with the fine perforated metal sheet mentioned above. This produces a smooth flow in and around the bleeding holes.

The photograph in Fig. 29 shows the test section from the side, as well as the traverse to move the probes. This traverse is driven by D.C. motors whose speed can be varied continuously. The local position of the traverse corresponds to the digital output of a position encoder. This digital signal is fed to a digital/analog converter which controls the X-Y-plotter to record the data. A direct analog voltage output of the traverse would have been simpler and cheaper, but the above described system was available. Nevertheless, also this comparatively accurate system was checked by dial gages on the traverse.

The measuring instruments are shown in Fig. 30. The little plexi-

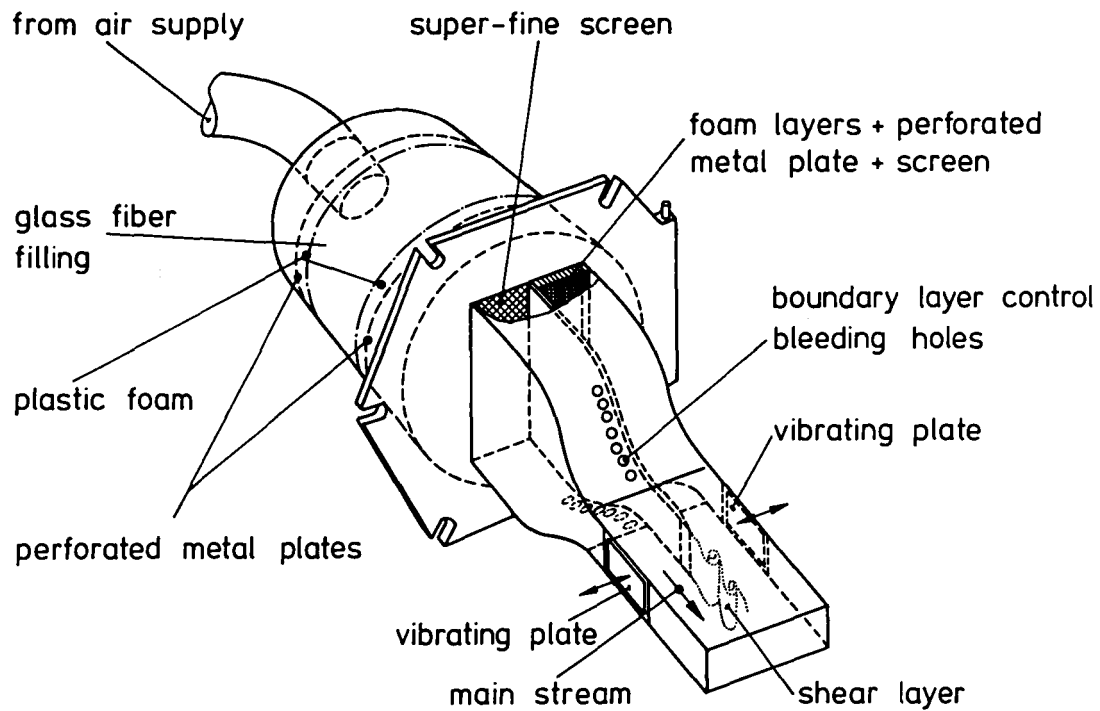


Fig. 27 Schematic view of the facility in Berlin.

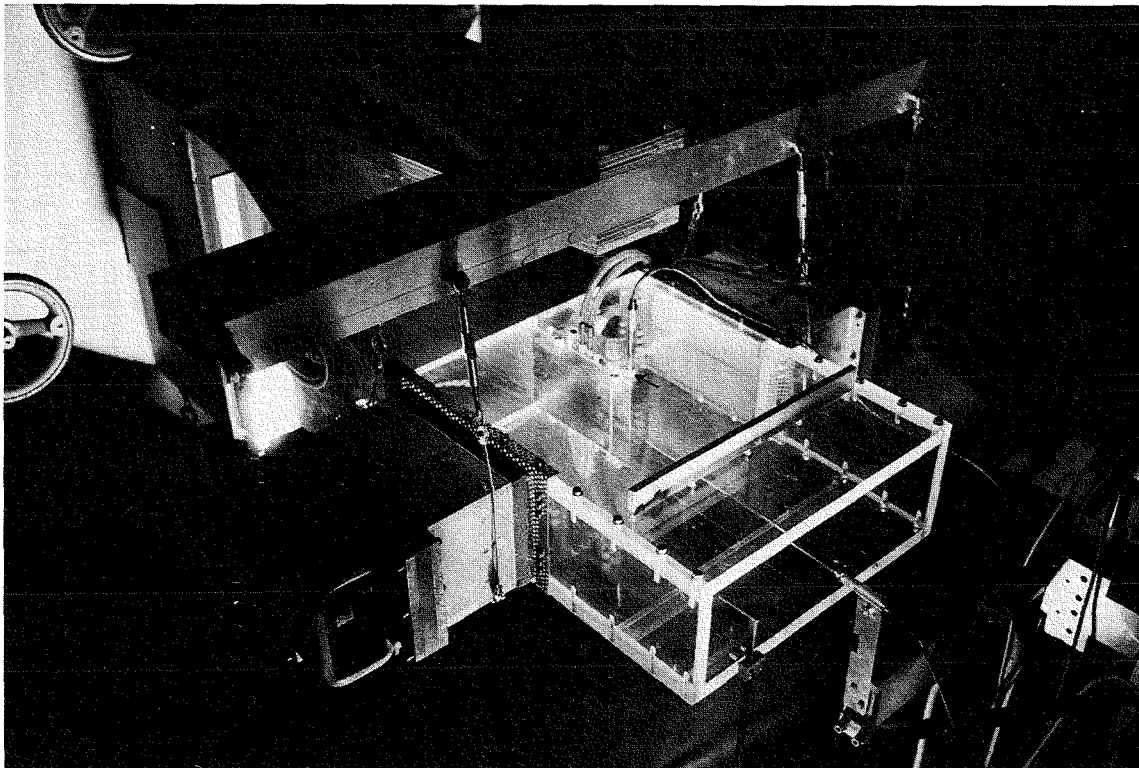


Fig. 28 Test section of the facility in Berlin with hot wire probe and a 1/4" condenser microphone (see arrow) in a position to measure p_1 near the splitter plate edge.

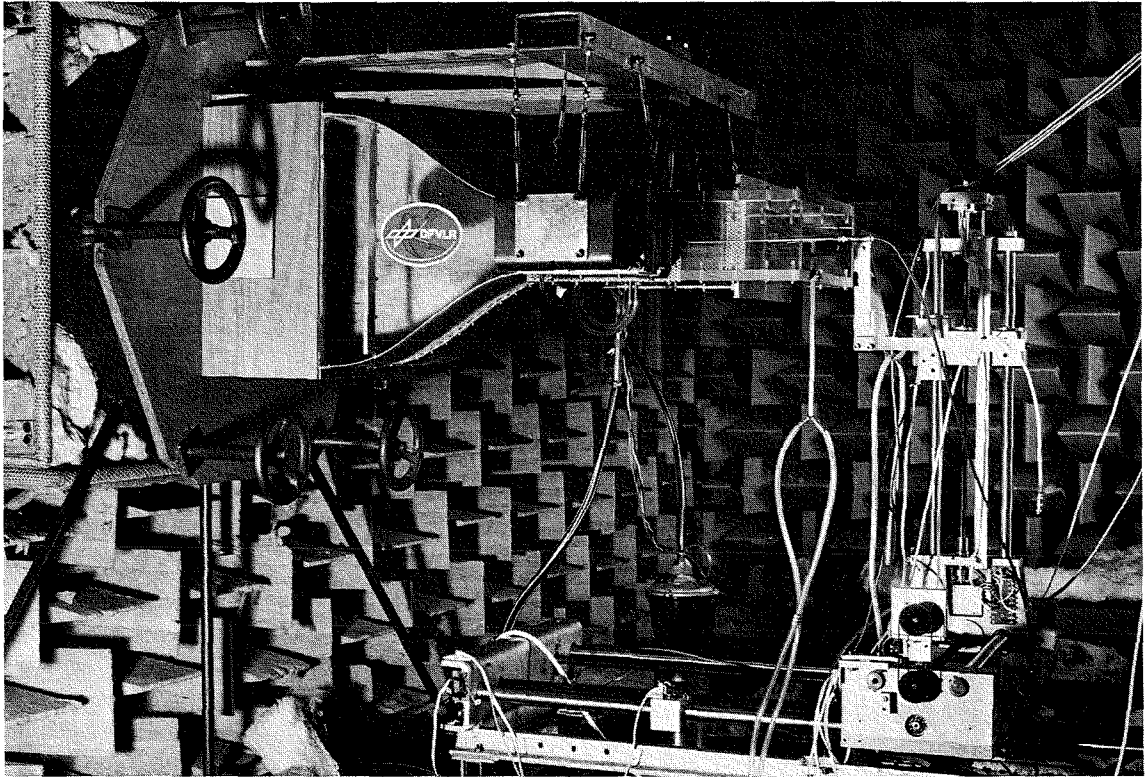


Fig. 29 Side view of the facility in Berlin with probe traverse.

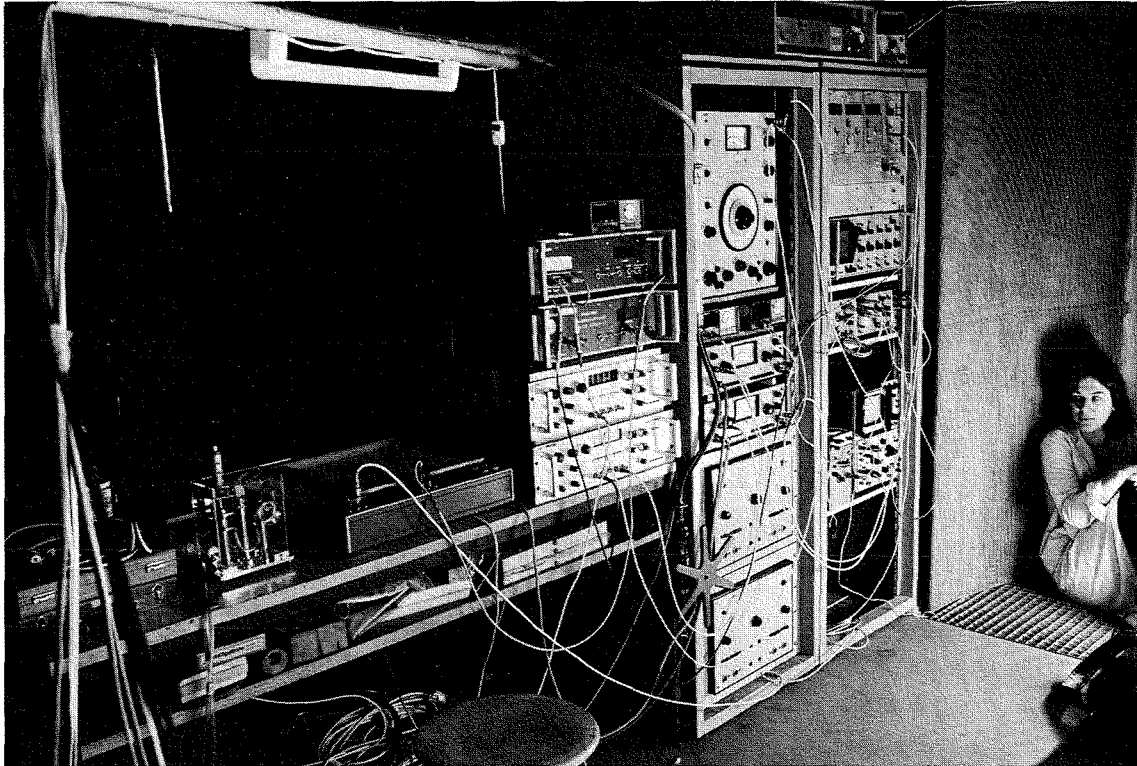


Fig. 30 Measuring instruments of the facility in Berlin.

glass box on the left hand side is the micromanometer (System Rechenberg) to measure the mean flow velocity with a pitot static tube. On the table we see also the X-Y-plotter which was used to record almost all data. The next pile of instruments to the right contains a little digital voltmeter on top for calibration and checking purposes. The two grey boxes below it are two phase meters *) (we would have needed only one, but both had little deficiencies and could be checked against each other). Below that, still on the table, are two hot wire anemometers, type DFVLR HDA III. In the first following rack we have from top to bottom: (a) a beat frequency oscillator to drive the sound excitation and the slave filters, (b) two voltmeters to monitor the driving voltage of the vibration plates of the sound excitation, (c) two B & K 2607 measuring amplifiers for microphone and hot wire signals. On top of the two racks we have the digital motor control and a little counter to measure the frequency of the excitation. The rack on the right hand side (closest to the girl) contains from above (a) the digital traverse control and the digital/analog converter for the spatial position signal of the traverse, (b) a four beam oscilloscope, (c) two power amplifiers with phase shift units for the vibrating plates of the acoustic excitation, (d) another amplifier and phase shift unit of the same type to control the piston speaker in the boundary layer suction duct, and (e) a two beam storage oscilloscope. For some of the measurements, i.e., the spectra, a Hewlett-Packard HP 5420 A Digital Signal Analyzer was used. Because its cooling fan is very noisy, it was kept outside the measuring room and is, therefore, not shown here.

*) We would like to stress here that it is very difficult indeed to carry out phase measurements in a flow. A phase meter will show an output signal under all circumstances, even if the reading is nonsense. A typical situation is this: An analog phase meter is exposed to a slightly jittering signal close to 0° or 360° ; the reading will be approximately 180° ! So the operation of the phase meters is to be checked carefully. One way to do this is to monitor the reference signal and the (rectangular) switching signal from the phase meter circuitry. Digital phase meters usually do not have this problem; on the other hand, they cannot be used in a simple way to produce a continuous data plot.

9.2.3. Boundary layer suction

The design of the boundary layer suction system can be seen in Figs. 31 and 32. Fig. 31 shows on the left hand side the splitter plate with the suction slit. The suction air passes through a diffuser inside the plate. The flow resistance of a plastic foam element enforces an equal velocity distribution over the slit cross section. Subsequently, the air is removed through two tubes on both sides of the plate (the Houston facility had only one tube on each side which caused little, but audible broad band flow noise at the tube inlets). The plastic hoses connecting the splitter plate cavity with the manifold (see Fig. 31) have equal length. On the right hand side of Fig. 31 we see the piston speaker to compensate the A.C. flow through the suction slit (See also Fig. 29). Both sides of the loudspeaker piston membrane are connected by a little pressure exchange hose to prevent damage from static pressure loading. To suppress acoustic resonances in the suction duct system, we use a long (30 m) garden hose as an anechoic termination. For the suction blower which we use, a normal vacuum cleaner and thus a tremendous noise source, we had to devise an excellent muffler. Our muffler (see Fig. 32) consists of an ordinary 200 l sheet metal barrel filled with plastic foam flakes of the kind which are normally used to fill pillows. In order to prevent the flakes from clogging the duct connections, coffee sifters covered with elastic lady's stockings are glued onto the inner side of both lids of the barrel. This muffler is very efficient and thus the suction air flow is inaudible.

The control valve and the flow meter (see Fig. 32) are downstream of the muffler because they also produce noise. The vacuum cleaner is located in another room (in a box in the Houston facility) to avoid noise contamination. For the air flux might be too low to provide the necessary inner cooling of the vacuum cleaner, a bypass air stream is ingested through a bypass valve (See Fig. 32). The suction volume flux was

Houston: 28.3 l/min
Berlin: 34.0 l/min .

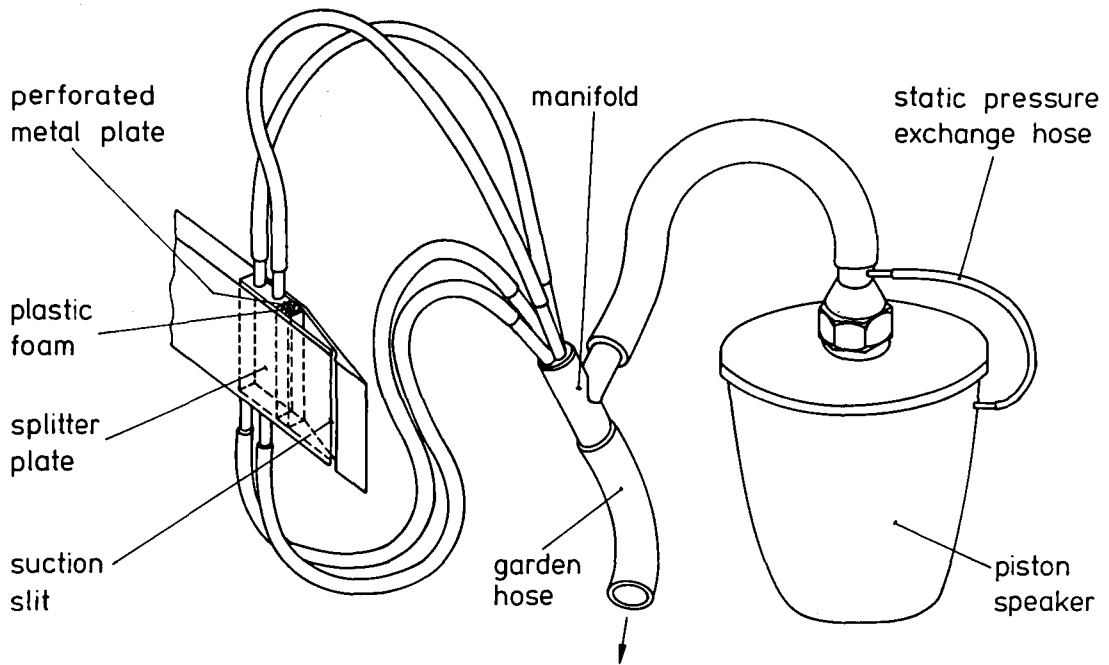


Fig. 31 Boundary layer suction: splitter plate, manifold and compensation piston speaker.

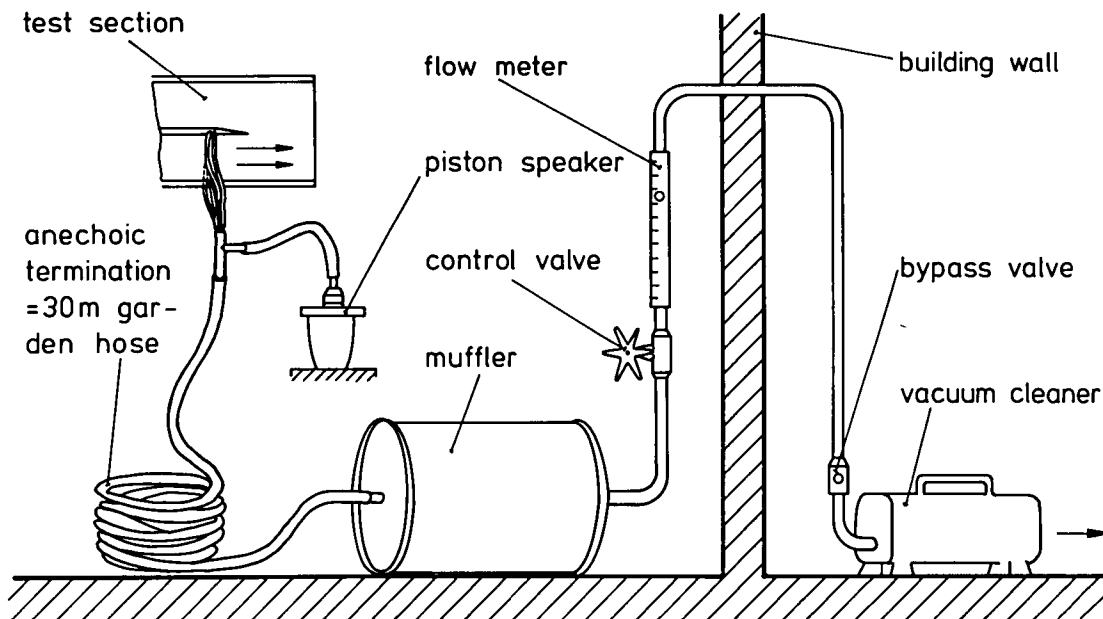


Fig. 32 Boundary layer suction: survey.

The slit width was 1.0 mm and the splitter plate breadth was 100 mm, in both facilities.

Finally, we should mention, that it turned out that the slit A.C. flow compensation with the compensation piston speaker had no perceivable effect on the shear layer excitation. This was most likely due to the high flow resistance of the foam element in the cavity of the splitter plate (see Fig. 31) and due to the suppression of resonance with the anechoic termination. Consequently, the slit A.C. flow compensation was after all not necessary and not used in our experiments.

9.2.4. Vibration system

The vibrating plates to produce the sound excitation were originally designed for another previous facility where the production of high sound levels was crucial [21, 22]. This system was used in both, the Houston and Berlin experiments. Its vibrating plates consist of a balsa wood sandwich structure (see Fig. 33), which leads to a very low mass (7 g). The lowest eigenfrequency of the plate was calculated to be above 200 Hz. The complete vibrating elements with coils and cast silicone rubber bellows can be seen in Fig. 34. They are mounted in an aluminium structure shown in Fig. 35. The coils operate in the magnetic field of two commercial loudspeaker magnets designed for 37.5 Watts power input each. The total possible power input of the systems would be then 150 Watts maximum. However, this high possible power is not used in our experiments, though it provides a considerable and safe linearity range. The magnitude limit is given in our low frequency range experiments by the maximum possible deflection of the plates which is ± 3 mm, but even this is by far not reached in any of our experiments. The low frequency response of the system is impressive; there is no problem to run the vibrating plates at, say, 10 Hz.

In the Berlin facility, the complete vibrating plate systems are suspended with steel ropes (see Fig. 28) and they are attached to the test section with a rubber foam frame. This suspension avoids vibrations from being fed into the test section. The vi-

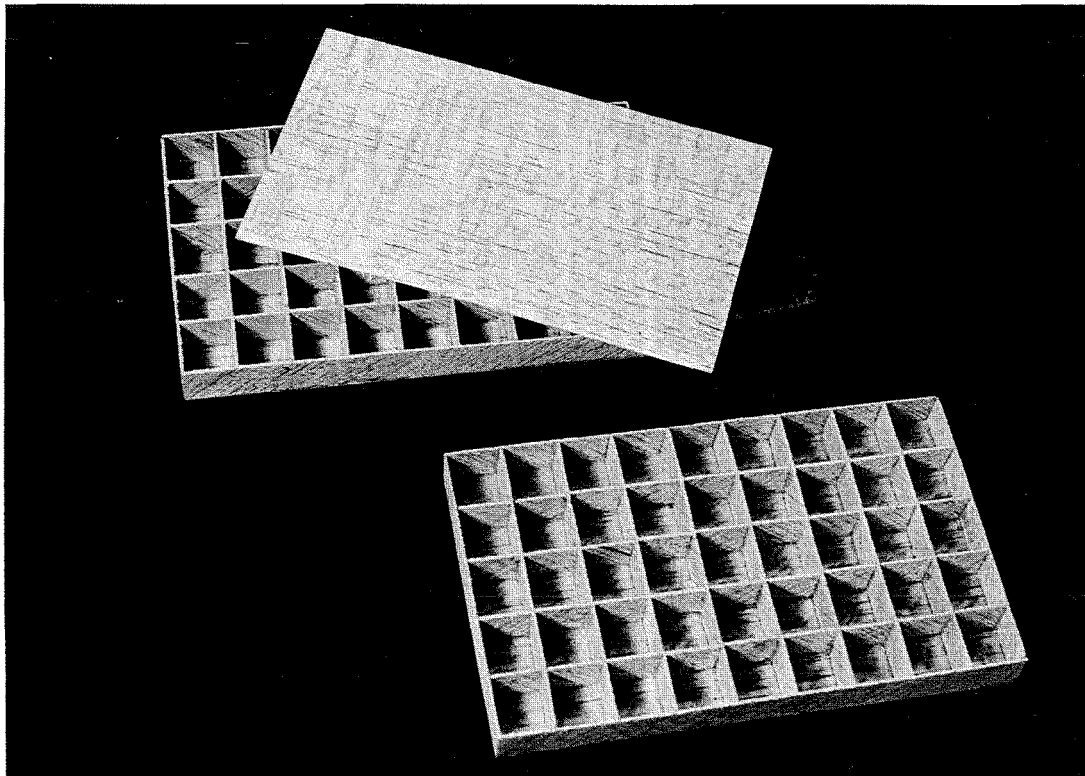


Fig. 33 Vibrating plates before being assembled. The sandwich structure is visible. Mass: 7 g each.

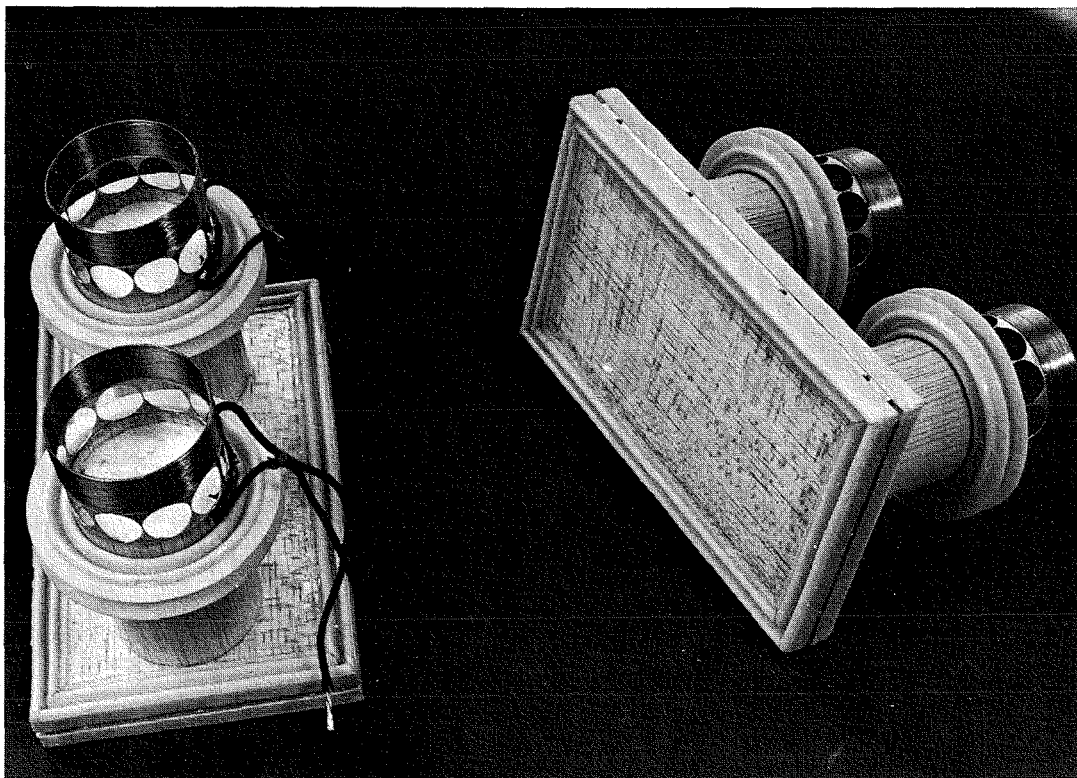


Fig. 34 Vibration units with coils and cast silicone rubber bellows suspensions. Mass: 60 g each. Maximal admitted acceleration: 3000 m/s^2 .

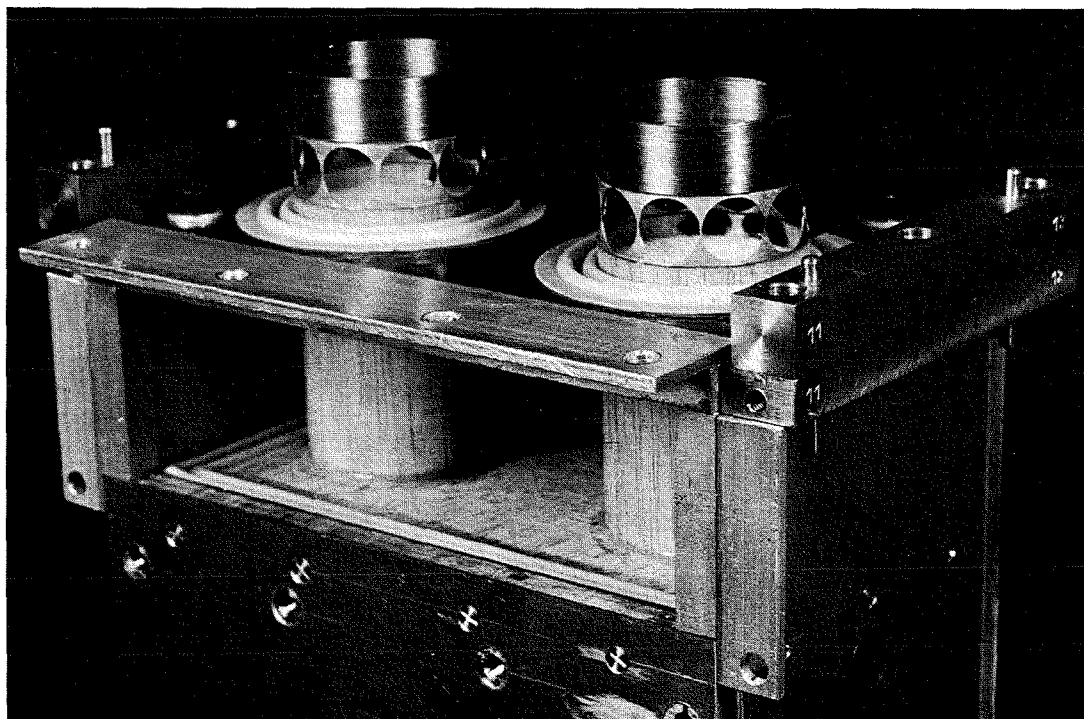


Fig. 35 Vibration system partly assembled, without magnets.

bration sensitivity of microphones is not appreciated widely and can lead to severe systematic errors. To give an example, Fig. 36 shows this sensitivity for a 1/4" Brüel & Kjaer microphone. The microphone is exposed to constant lateral acceleration of $0.1 \text{ g} = 0.98 \text{ m/s}^2$ at various frequencies. The vertical axis of the diagram shows the apparent sound pressure level. This test with a microphone mounted on a shaker is impressive but not very helpful in an experimental situation, because the vibration sensitivity varies from microphone to microphone and depends also on how the microphone is mounted. Moreover, it looks as if not only the microphone cartridge but also the adjacent preamplifier is sensitive to vibrations. A useful test for the actual contamination of the microphone signal is the following: A jacket for the microphone is attached to the test section wall close to the measuring location, but not connected to the inner part of the test section. If the microphone is plugged into that jacket under measuring conditions, it is only exposed to the vibration and not to the sound. Thus, the measured signal is representative for the contamination alone. It should be mentioned, that, obviously, the vibration contamination and the sound signal

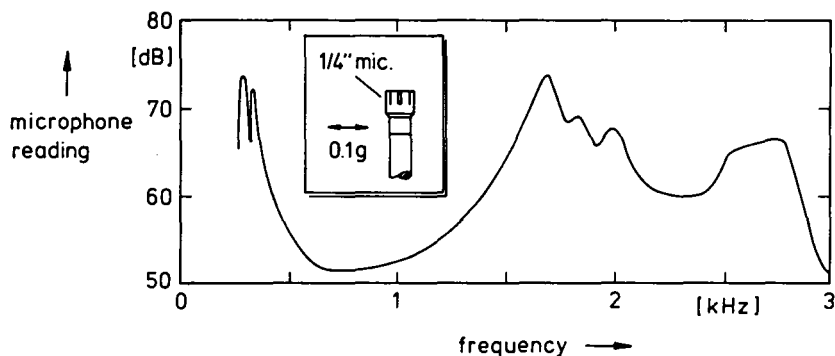


Fig. 36 Vibration sensitivity of 1/4" Brüel & Kjaer condenser microphone. The apparent sound pressure level is shown, if the microphone is exposed to a $0.1 \text{ g} = 0.98 \text{ m/s}^2$ acceleration at various frequencies.

are completely coherent. Consequently, if the vibration signal is, say, 20 dB lower than the sound signal, the vibration contamination error is still 10 %. Vibration contamination was a major error source in the Houston measurements, but the validity of the measurements was checked in each case with the test procedure described above. In the Berlin measurements, this error is completely eliminated due to the better suspension of the vibration systems.

Finally, we will comment on the electric adjustment of the vibrating plates. To produce an antisymmetric sound field *) the vibrating plates have to be adjusted in magnitude and phase. A magnitude adjustment is straight forward by the volume control of the amplifier. If one thinks of a phase adjustment, one thinks of an electronic circuit which changes the phase independent of the magnitude. This is comparatively difficult to achieve and, in fact, not necessary. If we insert a circuit as shown in Fig. 37 between oscillator and power amplifier we can change the

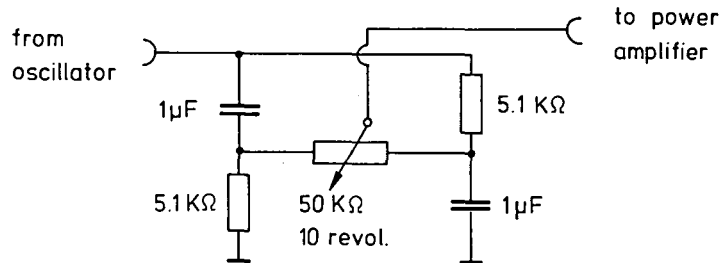


Fig. 37 Phase shift circuit for the adjustment of the vibration plates.

*) A shear layer excitation experiment does not really require an antisymmetric sound field; the relevant quantity is Δp_{12} which has to be measured accurately. However, the u-velocity field far outside the shear layer does depend on the excitation field and thus the similarity between available theoretical data and field measurements becomes closer, if the sound field is adjusted properly in the antisymmetric shape.

phase over a range of almost 180° , together with a moderate change in magnitude. Another $\pm 180^\circ$ phase shift can be obtained by inverting the vibration system voltage by a simple switch. With such a control circuit for both vibrating plates any conceivable phase relation between the plates can be produced. The adjustment is still straight forward with (a) volume control of the power amplifier, and (b) coupled phase/volume control of a phase control circuit as shown in Fig. 37. The procedure requires a few consecutive control steps on each knob and can be carried out in a few minutes. The quantity to become zero (or better, say, -60 dB below the original signal) is the probe microphone output on the symmetry line of the facility under no flow condition (see Fig. 12 in section 5).

9.2.5. Background noise

The most relevant information on background noise is in how far it contaminates our (filtered) measurements taken at one single frequency, chosen between say, 30 Hz and 200 Hz. Such data have been given already in section 6, referred to as "background noise" *). The authors claim to have established facilities with exceptionally low noise. So we have to contribute at least some data on this issue. We measured in our Berlin facility the following quantities:

- (a) level and spectrum of the excitation pressure difference
 $\Delta p_{12} = p_1 - p_2$ at a distance $l = 13$ mm upstream of the splitter plate edge
- (b) level and spectrum of the pressure p_2 alone, at the same location

*) The general term "turbulence level" does not make sense to the authors in the present context, because velocity fluctuations can be generated by both convected vorticity and by sound. In addition, the "turbulence level" depends crucially on the lower cut-off frequency of the measuring amplifiers and this cut-off frequency should be very low indeed.

(c) level and spectrum of the pressure p_s in the settling chamber.

The spectra are shown in Figs. 38 to 40, the filter bandwidth was 6.25 Hz. The sound pressure levels (2 Hz - 20 kHz) are shown in the following Table 1 *).

\bar{U}_2 [m/s]	Δp_{12} [dB]	p_2 [dB]	p_2 [dBA]	p_s [dB]
0	53.7	57.5	36.8	57
6	59.6	73.7	41.8	77.5
8.5	-	81.6	67.9	86.4
12	88.2	90.2	83	89.4
17	-	95.5	89.6	99.8

Table 1: Background noise, facility Berlin.

In all cases, in particular in the settling chamber, the low frequency constituents of the spectrum are dominating. A careful inspection of the spectra reveals some more details: The contamination from the mains supply (50 Hz and its multiples) is very low and does not exist in the settling chamber. This suggests, that the peaks measured in the test section are from the acoustical humming of the instruments rather than from electronic contamination. The background noise spectrum at $\bar{U}_2 = 0$ is very smooth, which suggests electronic noise rather than real acoustic background noise, except at the very low frequencies. The noise in the settling chamber at $\bar{U}_2 = 12$ m/s shows a regular pattern of broad humps. These are most likely not blower tones which would show up as sharp spikes. We think, it is the resonance pattern

*) The dB or dBA readings of measured pressures with broad band signals in this section refer to the RMS levels of these quantities, whereas in the previous chapters where we deal with sinusoidal signals, the quantities between vertical bars, like $|u|$, refer to the peak values of these quantities. The dBA reading differs from the dB reading, because in the dBA scale, the lower frequencies are more and more suppressed with decreasing frequencies. The dBA weighted scale was invented to simulate the sensitivity of the ear. For details see textbooks in acoustics, e.g., Beranek, Acoustic measurements [23].

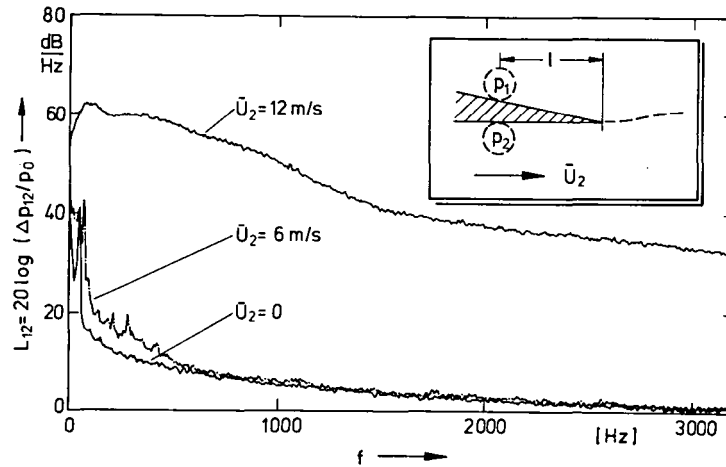


Fig. 38 Spectrum of the pressure difference Δp_{12} at both sides of the splitter plate (Berlin data). The distance from the plate edge is $\lambda = 13$ mm. The filter bandwidth is 6.25 Hz.

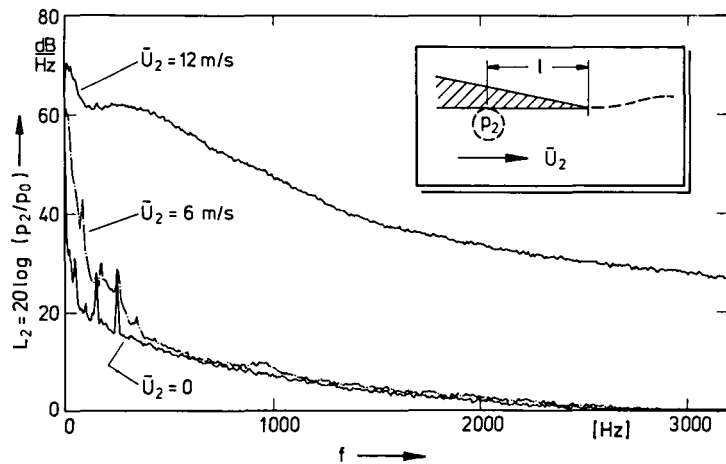


Fig. 39 Spectrum of the pressure p_2 near the edge of the splitter plate (Berlin data). $\lambda = 13$ mm. The filter bandwidth is 6.25 Hz.

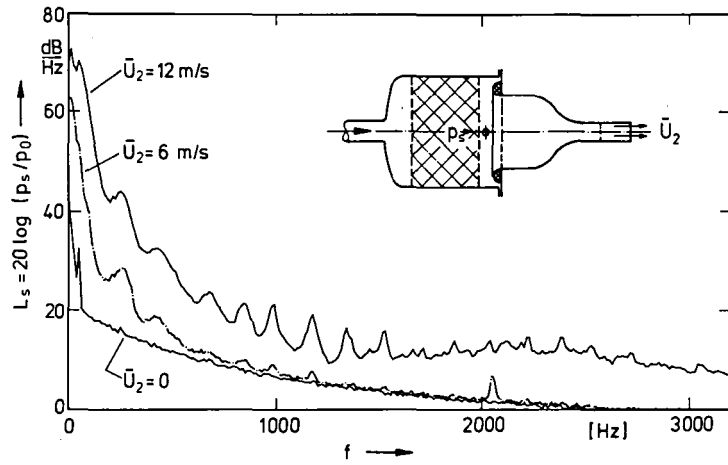


Fig. 40 Spectrum of the pressure p_s in the settling chamber (Berlin data). The filter bandwidth is 6.25 Hz.

of the air supply duct. We hesitate to speculate about the reasons for the very significant change in background excitation pressure level $\Delta p_{1,2}$ (see Fig. 38) between 6 m/s and 12 m/s. We would tend to attribute the very low frequencies, say, below 100 Hz, to the flow producing apparatus, i.e., everything upstream of the settling chamber, because at such low frequencies the mufflers do not work anymore. If we consider the broad band noise spectrum at 12 m/s (see Fig. 38), we see a maximum at about 300-400 Hz. We have no conclusive explanation for this, but one candidate is the observed incipient turbulence in the corners of the test section, to which the microphones are exposed. All these ramifications, however, are of minor importance, except the low frequency noise, which indeed causes trouble with the measurements.

For comparison, the Houston facility is much less documented; we have the following data (Table 2):

\bar{U}_2 [m/s]	p_2 [dB]	p_2 [dBA]
0	55	<43
8.5	81	57
17	91.5	77

Table 2: Background noise, facility Houston.

The dB measurements have been taken in the frequency range 10 Hz to 200 kHz. The dB to dBA relation suggests again dominating low frequencies. However, some measurements in Houston, in particular the phase measurements (see section 6.3.), were much more stable. This suggests, that the low frequency background contamination may have been in the order of 10 dB lower than in the Berlin facility, for identical operation conditions.

9.3. Appendix C

Typing errors of DFVLR-FB 82-23

"Excited Waves in Shear Layers" by D.W. Bechert

p. 22, line above eq. (34): ...is equivalent to $-\frac{1}{r} \cdot \frac{\partial p}{\partial \beta}$ at $\beta = \pi$

p. 30, eq. (60) is equal to zero.

p. 35, eq. (69) should read:

$$(69) \quad \left\{ \begin{array}{l} \tilde{u}_1 = \frac{\sqrt{\pi}}{4} \left[\frac{e^{\tilde{\lambda}_1 \tilde{x}}}{\sqrt{\tilde{\lambda}_1}} - \frac{e^{\tilde{\lambda}_2 \tilde{x}}}{\sqrt{\tilde{\lambda}_2}} \right] \\ \tilde{u}_2 = -\frac{i\sqrt{\pi}}{4} \left[\frac{e^{\tilde{\lambda}_1 \tilde{x}}}{\sqrt{\tilde{\lambda}_1}} + \frac{e^{\tilde{\lambda}_2 \tilde{x}}}{\sqrt{\tilde{\lambda}_2}} \right] \end{array} \right\} \quad \text{for } x > 0$$

p. 38, points P_1 and P_2 with capital letters in the text.

p. 44, Fig. 10: $|\tilde{u}_2|$ instead of $|u_2|$.

p. 48, eq. (91) should read:

$$(91) \quad \frac{x+r_0}{(x-x_0)^2+y_0^2} = \frac{1}{2} \left[\frac{\bar{T}}{x-z_0} + \frac{T}{x-\bar{z}_0} \right]$$

p. 50, eq. (96) should be multiplied by $e^{\lambda_1 x}$

p. 54, eq. (110), valid for $x > \bar{u}_0/\omega$

p. 73, footnote, ...at a frequency of 100 Hz;

p. 75, eq. (166) should read:

$$\Delta_{p12}/\sqrt{\ell} = \dots\dots$$

p. 112, eq. (135) should read:

$$(B5) \quad \left\{ \begin{array}{l} S_{\text{Re}} = \frac{\rho \omega^2 h}{2\theta} \cdot \frac{1}{\cosh^2(y/2\theta)} \\ S_{\text{Im}} = -\frac{\rho \omega^2 h}{2\theta} \cdot \frac{\tanh(y/2\theta)}{\cosh^2(y/2\theta)} \end{array} \right\}$$

p. 141, Table 3: There is no hint in the text that the "phase °" is indeed a phase lag, and the reference phase is the phase of the (vector) difference of the two pressures $P_1 - P_2 = \Delta P_{12}$.

End of Document